Monthly Notices of the ROYAL ASTRONOMICAL SOCIETY

MNRAS **501,** 6083–6102 (2021) doi:10.1093/mnras/staa3482
Advance Access publication 2020 November 10

Life after eruption VIII: The orbital periods of novae

I. Fuentes-Morales [1]★ C. Tappert,[1]★ M. Zorotovic,[1]★ N. Vogt,[1] E. C. Puebla,[1] M. R. Schreiber,[2,3] A. Ederoclite[4] and L. Schmidtobreick [5]

[1]*Instituto de Física y Astronomía, Universidad de Valparaíso, Avda. Gran Bretaña 1111, 2340000 Valparaíso, Chile*
[2]*Departamento de Física, Universidad Técnica Federico Santa María, Av. España 1680, 2340000 Valparaíso, Chile*
[3]*Millennium Nucleus for Planet Formation, NPF, 2340000 Valparaíso, Chile*
[4]*Instituto de Astronomia, Geofísica e Ciências Atmosféricas (IAG), Universidade de São Paulo (USP), Rua do Matão 1226, C. Universitária, 05508-090 São Paulo, Brazil*
[5]*European Southern Observatory, Casilla 19001, 7550000 Santiago 19, Chile*

Accepted 2020 November 4. Received 2020 November 4; in original form 2020 June 17

ABSTRACT

The impact of nova eruptions on the long-term evolution of Cataclysmic Variables (CVs) is one of the least understood and intensively discussed topics in the field. A crucial ingredient to improve with this would be to establish a large sample of post-novae with known properties, starting with the most easily accessible one, the orbital period. Here we report new orbital periods for six faint novae: X Cir (3.71 h), IL Nor (1.62 h), DY Pup (3.35 h), V363 Sgr (3.03 h), V2572 Sgr (3.75 h), and CQ Vel (2.7 h). We furthermore revise the periods for the old novae OY Ara, RS Car, V365 Car, V849 Oph, V728 Sco, WY Sge, XX Tau, and RW UMi. Using these new data and critically reviewing the trustworthiness of reported orbital periods of old novae in the literature, we establish an updated period distribution. We employ a binary-star evolution code to calculate a theoretical period distribution using both an empirical and the classical prescription for consequential angular momentum loss. In comparison with the observational data we find that both models especially fail to reproduce the peak in the 3–4 h range, suggesting that the angular momentum loss for CVs above the period gap is not totally understood.

Key words: accretion, accretion discs – novae, cataclysmic variables – techniques: photometric – techniques: radial velocities – techniques: spectroscopic.

1 INTRODUCTION

A nova eruption occurs in Cataclysmic Variable stars (CVs), which are close interacting binary systems composed of a donor, usually similar to a late-type main-sequence star, that fills its Roche lobe, transferring material to the white dwarf (WD) primary component. If the accumulated hydrogen on to low-luminosity WD reaches a critical value, a thermonuclear runaway (TNR) is triggered on the surface of the primary that ejects material into the interstellar medium. This process is known as a nova eruption and CVs that experienced such an event are called classical novae or post-novae. The binary is not destroyed by the nova eruption, allowing for the accretion process to start anew, which possibly occurs as early as within one or two years after the eruption (Retter & Leibowitz 1998). The typical length of this recurrence cycle is currently estimated to $\geq 10^4$ yr (Shara et al. 2012a; Schmidtobreick et al. 2015). This is thus not to be confused with the class of recurrent novae, which have much shorter recurrence cycles and stellar configurations that usually differ significantly from the main bulk of CVs.

It is still not clear whether the behaviour of the CV between two subsequent nova eruptions is largely defined by the eruption, e.g. with the latter causing the CV to switch between different states of mass-transfer rate ($\dot{M}$), or whether the CV is mainly unaffected by the eruption, e.g. a low $\dot{M}$ pre-nova would emerge as a low $\dot{M}$ post-nova, and likewise for high $\dot{M}$ systems. In the latter case, it would be the intrinsic properties of the CV that determine the length of the nova cycle, without interaction with the nova eruption itself.

The first of the above possibilities has been investigated in greater detail by Shara et al. (1986), leading to the postulation of the Hibernation model. There, the irradiation of the secondary star by the post-eruption heated WD causes the former to drive a very high $\dot{M}$ for a certain amount of time that gradually decreases as the WD cools down. Ultimately, this is supposed to lead to a detachment of the secondary star from its Roche lobe, thus stopping the transfer of material, and the system entering 'hibernation'. As a consequence, all post-novae should appear as high $\dot{M}$ CVs (so-called nova-likes) during the decades or centuries following an eruption, then undergo a gradual transition into a low-$\dot{M}$ state and a dwarf-nova behaviour. As of yet, there is no clear evidence in favour or against this scenario. The discovery of former dwarf nova V1213 Cen appearing to transition to a brighter state with a stable, high-luminosity disc after the nova eruption is in good agreement with what is predicted by hibernation (Mróz et al. 2016). However, it should be noted that the last observations of that study, about 7 yr after the eruption, still show the system in decline from the eruption with a significant slope >0.1 mag yr^{-1}, so it may well be that the object on a comparatively short time-scale returns to its dwarf-nova state. This would be similar to the case of V446 Her, that was found

★ E-mail: irma.fuentes@uv.cl (LF-M); claus.tappert@uv.cl (CT); monica.zorotovic@uv.cl (MZ)

to show dwarf-nova-like variability already about 30 yr after the nova eruption (Honeycutt, Robertson & Kafka 2011b). In a study of pre- and post-nova brightness of 30 novae, Collazzi et al. (2009) found that, while some objects present an increased luminosity after the eruption, most do not. Furthermore, Weight et al. (1994) found that $\dot{M}$ did not decline for at least 140 yr after the eruption contrary to what the hibernation model predicts. A recent study of the long-term behaviour of post-novae (Vogt et al. 2018) also concluded that any decrease in $\dot{M}$ must be at much longer time-scales than $\sim$200 yr.

An alternative explanation for the luminous accretion discs in post-novae was given by Schreiber, Gänsicke & Cannizzo (2000). There, the ionized state of the disc is caused by the WD irradiating the accretion disc, and not by an increased $\dot{M}$ from the secondary star. Depending on the size of the affected area in the disc, this would leave some outer parts in the disc in a non-ionized state, thus explaining the so-called stunted outbursts observed in some post-novae (e.g. Honeycutt, Robertson & Turner 1998). Tappert et al. (2013) indeed found evidence for the presence of an optically thick inner disc in one such object. In the same line, Schreiber & Gänsicke (2001) concluded that the irradiated disc by the hot post-erupted WD plays a crucial role on the evolution of post-novae, with the decline in brightness being a direct consequence of the decrease of irradiation of the disc due to the cooling of the WD rather than an effect of a decrease in $\dot{M}$ as was interpreted by Duerbeck (1992).

One possibility to investigate the validity of above scenarios is to compare the physical parameters of the post-novae with those of the overall CV population. Of those, the orbital period ($P_{\rm orb}$) is the most accessible one and also represents already a rough indicator of the state within the secular evolution of CVs (e.g. Knigge, Baraffe & Patterson 2011). A number of theoretical orbital period distributions of novae have been published (Diaz & Bruch 1997; Nelson, MacCannell & Dubeau 2004; Townsley & Bildsten 2005). However, for a proper comparison with the observed distribution, the latter needs to be made out of a sample of statistically significant size. The main problem related in general to the study of the post-nova population is that these are mostly very faint objects, requiring a significant amount of time on large telescopes to study them. Diaz & Bruch (1997) made the first observational period distribution of old novae from a sample of 28 novae with $P_{\rm orb} < 10$ h. Analysing the influence of certain observational selection effects, they found that those parameters have a little effect on the shape of the period distribution. They also suggested a correlation between the nova explosion amplitude and the orbital period. Warner (2002) analysed the period distribution using 50 orbital periods he qualified as reliable, indicating a concentration to 3.3 h, and noting a similarity to a pile-up of magnetic CVs near this value. Townsley & Bildsten (2005) used that period distribution to show that their simulations are consistent with the idea that CVs evolve across the period gap. Tappert et al. (2013) compared the period distribution of all CVs (data from Ritter & Kolb 2003a, version 7.20, 2013) with 78 orbital periods of post-novae. They confirmed the concentration of novae at 3–5 h, in striking difference to the distribution of all CVs. This particular range is dominated by high mass-transfer systems (Rodríguez-Gil et al. 2007), in contrast to the general CV population, which is dominated by low-mass transfer and systems with orbital periods < 2 h (Pala et al. 2020). These differences were predicted by Townsley & Bildsten (2005) and likely reflect the shorter nova eruption recurrence times for high-mass transfer systems.

However, the period distribution of novae is both still under-sampled in large parts of the period range, such that an addition of a comparatively low number of new periods has the potential to significantly change the shape of the distribution. Therefore, any comparison with the predicted distribution will suffer from large uncertainties. This is the more important, because, since the brightness of the post-nova is mainly determined by the brightness of the accretion disc, the observed period distribution is potentially biased towards bright, long-period systems with high mass-transfer rates and low nova eruption amplitudes. Thus, short-period low mass-transfer novae could still amount to a significant number, but are hidden, because they are intrinsically faint. The work by Gänsicke et al. (2009) shows that observations of faint CVs are crucial for our understanding of CV evolution and the use of the period distribution as a diagnostic tool, and this likely is also the case for novae.

In this work, we derive the orbital period for a number of faint post-novae, and to improve the precision of already established periods for mostly eclipsing systems that were included in Vogt et al. (2018). Furthermore, the theoretically predicted period distribution of novae based on a binary population model is calculated and compared to the observational data.

2 OBSERVATIONS AND DATA REDUCTION

2.1 Photometric data

We obtained time-series photometry in the *V*-band in 2013, 2014, and 2015 using direct CCD imaging with a field of view of 8.85 arcmin square, 0.259 arcsec pixel scale, and a 2 × 2 binning at the 2.5-m du Pont telescope at Las Campanas Observatory, Chile. Alignment of the individual images for each field was performed by the ASTROIMAGEJ software (Collins et al. 2017). All fields were reduced by bias and flat-field correction and instrumental magnitudes were calculated with aperture photometry using the DAOPHOT package from IRAF. The aperture radius in each frame was adopted as the average of the full width at half maximum (FWHM) of the stellar point spread function (PSF) in a given frame. Differential magnitudes were calculated using comparison stars in the vicinity of the post-nova, within a radius of 400 pixels. In order to calibrate the instrumental magnitude, stars with known *V* magnitude were chosen to be compared with their tabulated *V* magnitudes either in the Naval Observatory Merged Astrometric Data set (NOMAD; Zacharias et al. 2004) or in the GSC (The *HST* Guide Star Catalogue, version 2.3.2) catalogue. The calculated *V* magnitudes are presented in the log of observations (Table 1).

Further *V*-band data were obtained between 2013 August and 2015 August with A novel Double-Imaging CAMera (ANDICAM) placed at the 1.3-m telescope operated by the Small and Moderate Aperture Research Telescope System (SMARTS) consortium, at the Cerro Tololo Inter-American Observatory (CTIO), located in La Serena, Chile. The field of view was 6 arcmin square and we used a 2 × 2 binning. These observations yielded differential photometry over a time range of 2 yr with a time resolution of the order of 3–5 d. For more details concerning these data see Vogt et al. (2018, paper VII). Hereafter we refer to these observations as 'CTIO set'.

2.2 Spectroscopic data

Time-series spectroscopic data were collected from the following observing runs: with the ESO Faint Object Spectrograph and Camera (EFOSC2; Buzzoni et al. 1984) at the ESO New Technology Telescope (NTT) in La Silla, Chile, we obtained data in 2011 June/July, 2012, and 2013 May. The grism used was #20 covering a wavelength range of 6040–7140 Å with a 1 arcsec slit, yielding a

Table 1. Log of observations. Above: time-series photometry. Bottom: time-series spectroscopy. *N* refers to the number of observations, t_{exp} is the exposure time in seconds, Δt is the time covered by observation in hours. Last column contains the magnitude value and the bandpass which it was measured. For the CTIO data, see Vogt et al. (2018).

Object	Date	*N*	t_{exp}	Δt	Magnitude
X Cir	2015-05-19	209	60	7.93	18.77(32)*V*
	2015-05-20	80	60	2.89	18.76(38)*V*
	2015-05-21	56	60	1.99	18.82(33)*V*
	2015-05-23	37	60	1.48	18.81(37)*V*
	2015-07-10	66	90	3.33	19.04(23)*V*
IL Nor	2015-05-20	100	60	3.77	18.73(07)*V*
	2015-05-21	53	60	1.89	18.52(07)*V*
	2015-05-22	39	180	2.74	18.48(04)*V*
	2015-05-23	42	60	1.66	18.24(07)*V*
DY Pup	2013-12-31	139	90	5.11	19.16(07)*V*
	2014-01-01	47	60	1.66	19.14(07)*V*
V2572 Sgr	2012-05-16	142	40	3.15	17.92(08)*V*
	2015-05-20	79	60	2.88	17.65(14)*V*
	2015-05-21	121	60	4.36	17.77(10)*V*
	2015-05-22	167	60	6.15	17.73(19)*V*
	2015-05-24	90	60	3.34	17.68(08)*V*
	2015-07-11	52	60	2.78	17.81(10)*V*
XX Tau	2013-12-28	128	60	4.62	19.11(08)*V*
	2013-12-30	45	60	1.59	19.15(09)*V*
	2013-12-31	37	60	1.31	19.11(08)*V*
	2014-01-01	18	120	0.92	19.05(07)*V*
CQ Vel	2013-12-28	55	120	2.88	19.13(12)*V*
	2013-12-29	79	120	5.37	19.05(11)*V*
	2013-12-30	115	120	6.00	19.00(08)*V*
	2013-12-31	22	120	1.12	18.99(08)*V*
	2014-01-01	99	120	5.17	19.11(07)*V*
V2572 Sgr	2011-06-29	1	900	0.25	18.30(59)*R*
	2011-06-30	3	900	3.54	18.52(15)*R*
	2011-07-01	8	900	9.39	18.46(05)*R*
	2011-07-03	1	900	0.25	18.64(10)*R*
XX Tau	2018-12-30	8	600	0.90	–
	2018-12-31	6	600	1.17	–
	2019-01-01	20	600	3.72	–
	2019-02-10	4	600	0.91	–
	2019-02-12	4	600	0.91	–
RW UMi	2015-06-19	10	600	1.56	–
	2015-06-21	16	600	2.60	–
	2015-06-22	5	600	0.69	–
CQ Vel	2012-03-25	2	900	0.70	19.57(04)*R*
	2012-03-26	9	900	3.39	19.36(04)*R*
	2012-03-27	7	900	2.69	19.35(28)*R*

resolution of 3.7 Å. In 2018 December and 2019 January, additional data on XX Tau were obtained at the Very Large Telescope (VLT) using the FOcal Reducer/low dispersion Spectrograph 2 (FORS2; Appenzeller et al. 1998) with the 1200R grism and a 0.7-arcsec slit, covering a wavelength range of 5750–7319 Å with a resolution of 2.14 Å. Acquisition frames were taken with the edge filter *GG*435, thus no broad-band photometric magnitudes are available for this run. The nova RW UMi was observed in 2015 June with the Gran Telescopio Canarias (GTC), installed in the Spanish Observatorio del Roque de los Muchachos of the Instituto de Astrofísica de Canarias, in the island of La Palma, using the Optical System for Imaging and low-Intermediate-Resolution Integrated Spectroscopy (OSIRIS; Cepa 1998). The R2500R volume-phased holographic grating was employed, covering a wavelength range of 5575–7685 Å. A 0.6 arcsec slit yielded a spectral resolution of 2.5 Å, measured as the FWHM of the night-sky spectral lines. No acquisition frames were available, thus no estimates can be given for the photometric brightness of the object at the time of the observations.

The reduction and calibration of the data was conducted with IRAF. Reduction of the spectra consisted in bias and overscan subtraction and division by a flat-field that had been normalized by fitting a cubic spline of high order. The cosmic rays removal was performed with the LACOS_SPEC task for IRAF (van Dokkum 2001). 1D spectra were extracted with the APALL routine within the ONEDSPEC package. Wavelength calibration was determined with He, Ar, and Ne lamp for data sets. The spectra were normalized with respect to the continuum and corrected to heliocentric velocity with the IRAF's RVCORRECT task.

2.3 Periodicity search

While CVs are known for the presence of strong emission lines in their spectra, among whose Hα is usually the most prominent one, most post-novae actually show comparatively weak emission lines (e.g. Tappert et al. 2014, and references therein), indicative of an optically thick accretion disc and a high mass-transfer rate. Additionally, most spectroscopic targets of this study proved to be rather faint ($V > 18.0$), and thus the best signal-to-noise values did not exceed 5 and 10 for the EFOSC2 and the FORS2 data, respectively. This, together with most lines being broad, asymmetric, and of variable shape, rendered the usual methods of fitting the line profile to measure its Doppler shift unsuccessful. Thus, the technique used by Tappert et al. (2013) to measure the Hα displacement was employed: First, each normalized spectrum was smoothed down to the effective spectral resolution of the instrument. Secondly, to account for potential imperfections related to the wavelength calibration, individual wavelength corrections were applied with respect to the λ6300.304 Å [O I] sky emission line. Subsequently, the average spectrum for each target was cross-correlated by eye to each individual spectrum by applying a positional shift and an intensity scale factor. The resulting displacement was recorded as the radial velocity shift.

The periodicity analysis in both light curves and radial velocities was performed with PERANSO (Paunzen & Vanmunster 2016), which allows us to choose among different methods based on discrete Fourier transform algorithm. The Lomb-Scargle routine was used and the error was estimated as the frequency resolution in each campaign. i.e. $1/\Delta t$.

Radial velocities are fitted with a sinusoidal function as

$$v_r(t) = \gamma + K \sin[2\pi (t - T_0)/P_{orb}], \quad (1)$$

where $v_r(t)$ is the measured radial velocity at time t, K corresponds to the semi-amplitude, γ is the systemic velocity, T_0 is the chosen zero-point, and P_{orb} is the orbital period of the system.

3 RESULTS

3.1 RS Car (1895)

This nova flared up in 1895 being discovered by Mrs. Fleming on photographic plates taken at the Arequipa Station of the Observatory (Pickering 1895). The maximum light was reported at photographic magnitude $m_{pg} = 7.2^m$. It was categorized as a slow nova and it was spectroscopically recovered by Bianchini et al. (2001) 7 arcsec away from the published position. The spectrum exhibited a blue continuum and an SED typically of an optically thick disc indicating that the system is still in a high-mass transfer state. Woudt & Warner

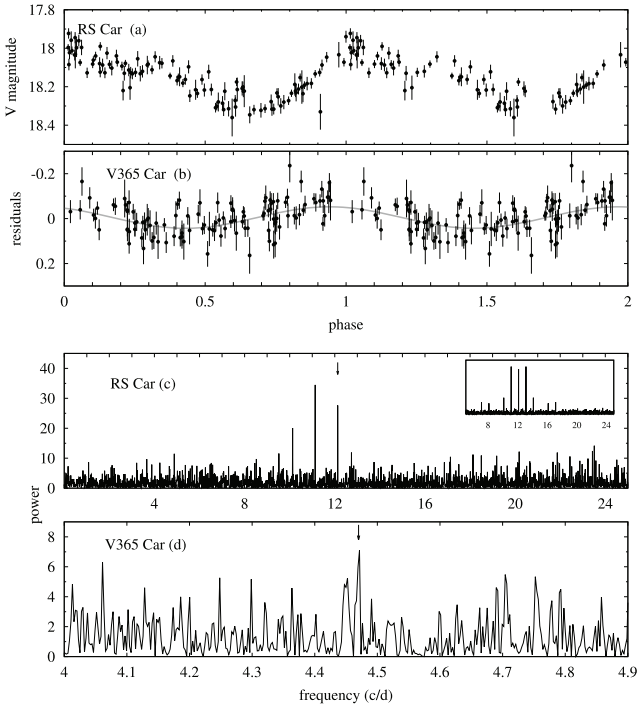

Figure 1. Phased light curves for (a) RS Car and (b) V365 Car according to ephemerides (2) and (4), respectively. (c) Scargle periodogram for RS Car and the spectral window centred at the frequency marked with an arrow. (d) the same for V365 Car in the range of the frequency found by Tappert et al. (2013). The arrow marks the peak at $f = 4.47$ c/d.

(2002) presented high-speed photometry in white light of this nova, exhibiting a light curve with several features resembling strong flickering. While they do not present a plot of the Fourier spectrum, they describe it as consisting of a strong signal corresponding to $P = 1.977$ h, i.e. 0.08238 d, and its harmonics. They ascribe this period to likely correspond to a superhump, based on RS Car showing the spectroscopic signatures of a high mass-transfer rate, which, at such short a period, is expected to produce an eccentric accretion disc, the latter being thought to be the physical reason behind the superhump signal (e.g. Wood et al. 2011). From our CTIO data, the periodogram presents two strong peaks at $f_1 = 11.13(01)$ and $f_2 = 12.13(01)$ c/d (Fig. 1c). The frequency resolution of the data set, $1/\Delta t$, was used to estimate the associated uncertainty. We note that f_2 corresponds to a period that is very close to the signal detected by Woudt & Warner (2002), implying that it is stable in time. We thus choose this as the main signal, in spite of it being the slightly lower of the two main peaks. Unfortunately, from the lack of corresponding information in Warner (2002), we cannot examine the possible presence of f_1 in their data. Taking the maximum of the modulation according to f_2 as zero-point, the ephemeris is

$$\mathrm{HJD(max)} = 2\,456\,676.7876(09) + 0^{\mathrm{d}}.082429(25)\ \mathrm{E}, \quad (2)$$

and the alternative ephemeris to f_1 is

$$\mathrm{HJD(max)} = 2\,456\,663.7723(16) + 0^{\mathrm{d}}.089842(81)\ \mathrm{E}. \quad (3)$$

The phased light curves using the ephemeris (2) are shown in Fig. 1(a). We note that the light curve shows similar characteristics as the one from Woudt & Warner (2002), but the sequence of the humps has been inverted, with the large hump now following the minimum, and the small hump being the one preceding it. Other differences are that the minimum appears to be slightly broader (by about 0.1 phases) and that the total amplitude with $\sim 0.3^{\mathrm{m}}$ is slightly larger.

3.2 V365 Car (1948)

This nova with an eruption in 1948, discovered by Henize (1967), has been largely described by Tappert et al. (2013), who performed both radial velocities and *R*-band photometry. They found a periodicity to $P = 0.2247(40)$ d and their light curve present a sinusoid or hump shape with an amplitude of $\sim 0.2^{\mathrm{m}}$. The CTIO data on V365 Car showed a long-term decline in brightness (see Vogt et al. 2018, for more details). After subtracting this trend, we performed a period search on the residuals. While the resulting periodogram does not present any obvious dominant signal, a closer look at the frequency range near the previously reported value of $f = 4.45$ c/d by Tappert et al. (2013) shows a narrow feature at $f = 4.4704$ c/d that rises slightly above the background noise (see Fig. 1d). Consequently, with the CTIO data was possible to refine the orbital period value. The improved ephemeris of the maxima is

$$\mathrm{HJD(max)} = 2\,456\,628.845(78) + 0^{\mathrm{d}}.22369(12)\ \mathrm{E}. \quad (4)$$

The folded light curve according to this period is shown in Fig. 1(b). Its shape as a sinusoid is similar to the one presented by Tappert et al. (2013), with an average amplitude of $\sim 0.1^{\mathrm{m}}$.

3.3 X Cir (1927)

X Cir underwent a nova eruption in 1927 (Becker 1929) and the position of the post-nova was recovered by Tappert et al. (2014). The spectrum indicated the presence of an accretion disc seen at high inclination, and the prominent Balmer emission lines along with a flat continuum point to low mass-transfer rate.

Special care was taken to perform the *V*-band photometry of this object, since a close visual companion is located at a distance of 0.8 arcsec southwestwards. To assure a clean background subtraction and to account for the different seeing conditions, the aperture photometry was performed using a large annulus that covered both components of the visual binary. In good agreement with the conclusions drawn from the spectroscopic appearance, X Cir turned out to be an eclipsing CV with $P_{\mathrm{orb}} = 3.71$ h. The light curves are shown in Fig. 2. A smooth variability is seen outside of the eclipse. The depth of the eclipse is slightly different in each cycle, varying from 1 mag to 1.5 over the seven observed cycles. At this stage it remains unclear whether these variations are intrinsic, or are caused by the presence of the companion in the aperture radius in combination with variable seeing.

X Cir was also part of the CTIO data set described in Vogt et al. (2018), although it is not included in that paper, for reasons stated below. The data consist of 96 frames with typically two subsequent exposures per night with integration times of 170 and 340 s. The set spans a time range of 168.7 d, from HJD 2 456 690.7934 to 2 456 859.5209. Basic reduction was performed as for the other objects of the CTIO data. However, because of the close companion, in combination with very variable seeing conditions, it was necessary to perform the aperture photometry of this object without applying a centring algorithm. For this purpose, one image frame with good seeing conditions was selected, and the positions of X Cir and the other component of the visual binary (hereafter M2) were measured with respect to a number of reference stars. In all other frames, the positions of those two components were calculated corresponding to the average of the shift of those reference stars with respect to the initially selected frame. Aperture photometry was performed at

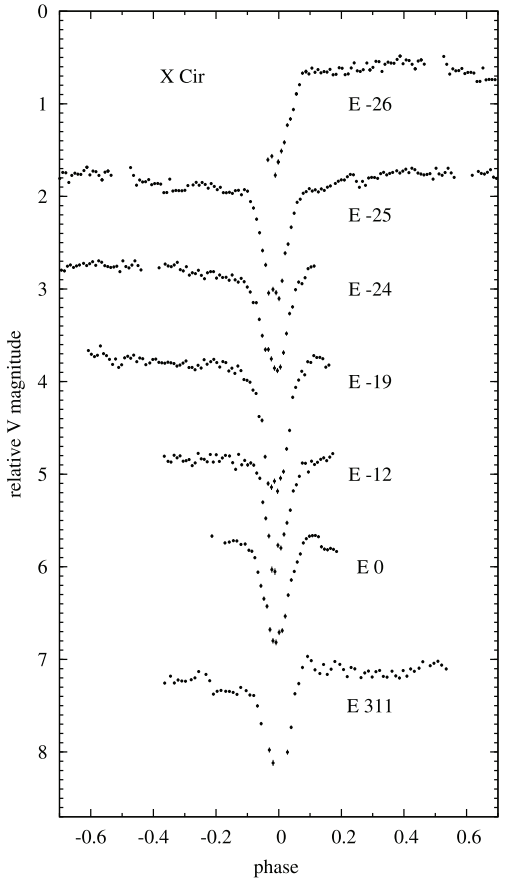

Figure 2. X Cir light curves from the du Pont telescope phased with the ephemeris (5). Each light curve was vertically shifted by 1.2 mag for the purpose of a clearer presentation.

the such defined positions, and additionally of one comparison star whose constant brightness had been previously established. Finally, the differential magnitudes of the post-nova were computed as the difference between the brightness measured at its position and the average of the values of the comparison star and M2. The resulting data are shown in Fig. A2 top. While it turned out that this light curve is still too strongly affected by the variable seeing to be used for a study of the intrinsic long-time behaviour of the post-nova, the fact that the data coverage includes a number of eclipses still made the set useful to refine above value of the orbital period obtained from the du Pont observations.

From the light curve, we identified 12 data points that could be unambiguously assigned to being part of an eclipse. Whenever there were two data points within the same night, we chose the fainter one as the time of eclipse, and in the cases where the two had identical brightness within the photometric uncertainty, we computed the average of those times. In order to calculate the correct cycles corresponding to each data point, we adjusted the orbital period iteratively. The value derived from the du Pont data was used to calculate the cycle corresponding to the second data point. A linear fit then yielded an improved period that was subsequently used to calculate the cycle corresponding to the third data point, and so forth. The fit to all six data points yielded $P_{\rm orb} = 0.154\,4504(38)$ d, which served to bridge the cycle count gap between the du Pont and the CTIO data, and allowed for an unambiguous cycle count in the latter

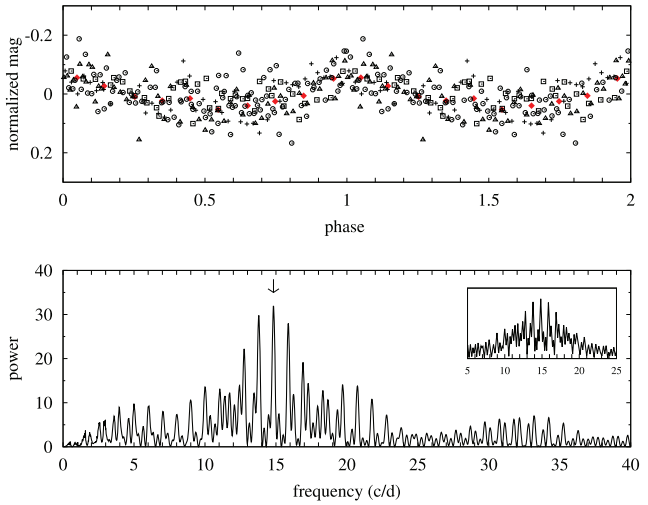

Figure 3. Top: Phased light curve for IL Nor according to ephemeris (6). The y-axis corresponds to the normalized V magnitude and the x-axis gives two orbital cycles in phase units. Different symbols indicate data from different nights. The red diamonds represent the average into 0.1 phase bins. Bottom: Periodogram of the photometric data. The arrow marks the highest peak, corresponding to $f = 14.83$ c/d. The inset shows the spectral window.

data set. The final fit to all eclipses gives the following ephemeris

$$\mathrm{HJD(min)} = 2\,457\,166.5047(12) + 0^{\rm d}.154\,459\,53(63)\,\mathrm{E}\,, \qquad (5)$$

where we chose the cycle number of the best defined of the most recent eclipse measurements as zero-point. The cycles, the measured eclipse times, and the fit residuals are given in Table 2, and the CTIO phased light curve folded with this ephemeris is shown in the bottom plot of Fig. A2. We ascribe the noisy eclipse shape and the light curve in general to the already mentioned different seeing conditions that caused a variable amount of the light of the close companion to be included in the aperture.

3.4 IL Nor (1893)

This is the oldest nova in the sample of new orbital periods, with an eruption reported in 1893 by Fleming and published by Pickering (1893). It was identified by Woudt & Warner (2010) based on photometric variability and spectroscopically confirmed by Tappert et al. (2012). The spectrum is dominated by weak emission lines and a blue continuum, indicating equal to RS Car that, more than one hundred years after the eruption this object still is a high mass transfer rate system. Photometry made by us (see Fig. A4) at du Pont revealed strong short-term variability with an average V magnitude of $18.5^{\rm m}$. In order to perform a period analysis, the V magnitude was normalized with respect to the mean of each night. The periodogram (Fig. 3 bottom) shows a signal at $f_1 = 14.83$ c/d and strong aliases at $f_2 = 13.80$ c/d and $f_3 = 15.87$ c/d which, if attributed to orbital modulation, correspond to $P_{\rm orb1} = 1.62(04)$ h, $P_{\rm orb2} = 1.74(04)$ h, and $P_{\rm orb3} = 1.51(03)$ h, respectively. Folding the data according to the alias frequencies does not present any significant differences with respect to the strongest peak. A comparison with the light curves of Woudt & Warner (2010) does not resolve this ambiguity either. However, from the spectral window (Fig. 3 bottom) it is evident that those peaks correspond to one cycle per day aliases. Considering the central peak in Fig. 3 at f_1, the ephemeris is

$$\mathrm{HJD(max)} = 2\,457\,163.639(09) + 0^{\rm d}.0674(15)\,\mathrm{E}, \qquad (6)$$

and for f_2 and f_3 the ephemerides are

$$\mathrm{HJD(max)} = 2\,457\,163.643(07) + 0^{\mathrm{d}}.0724(15)\ \mathrm{E}. \quad (7)$$

$$\mathrm{HJD(max)} = 2\,457\,163.642(05) + 0^{\mathrm{d}}.0630(15)\ \mathrm{E}. \quad (8)$$

The phased light curve folded to ephemeris (6) together with its orbital phase averaged into 0.1 phase bins are shown in Fig. 3 (top) and could correspond to the orbital hump of IL Nor with a total amplitude $\sim 0.1^{\mathrm{m}}$. At least the two neighbouring aliases mentioned above are also possible period solutions, requiring additional photometric and perhaps spectroscopic observations in order to decide which of the aliases is the valid one. In any case IL Nor turns out to be one of the very few classical novae below the period gap and is also the oldest confirmed nova among those short period systems.

3.5 DY Pup (1902)

The nova eruption was discovered in 1902 November 19 on Harvard plates, being reported by Shapley (1921), who established the photographic magnitude at maximum $m_{\mathrm{pg}} = 7^{\mathrm{m}}$. He also found that the pre-nova had $m_{\mathrm{pg}} > 10.3^{\mathrm{m}}$, and that must have been fainter than 16^{m} in 1901, because a photograph made in 1901 showing stars fainter than 16^{m} did not reveal any object at the nova position. DY Pup is catalogued as a slow nova considering the time it takes the brightness to decay by three magnitudes from maximum, i.e. $t_3 = 160$ d (Duerbeck 1987). The nova shell remnant is still visible and it was detected by Gill & O'Brien (1998) in 1995 as a ellipse-shaped remnant with a size of 7×5 arcsec. Despite its detection, the distance could not be estimated due to the lack of information on the expansion velocities. Comparison of the finding chart in Downes et al. (2005) and the images of the Panoramic Survey Telescope and Rapid Response System (Pan-STARRS; Chambers et al. 2016; Flewelling et al. 2020) unambiguously identifies DY Pup with a source in the *Gaia* Data Release 2 catalogue (Gaia Collaboration 2018). However, the measured parallax is 0.26 ± 0.31 mas, and thus presents an uncertainty that is too large for a meaningful distance determination (Bailer-Jones 2015; Schaefer 2018; Tappert et al. 2020).

Only two spectral observations have been reported (Zwitter & Munari 1994; Tomov et al. 2015). Both spectra are dominated by a blue continuum and weak H α emission line. In a poster presentation, and in a later proceeding, Van Zyl reported that DY Pup is an eclipsing system with $P_{\mathrm{orb}} = 3.35$ h (Downes et al. 2001; Warner 2003b), but the corresponding light curves were not published. Our V photometric observations confirm this information, detecting three eclipses during our two nights of observations (Fig. 4, Table 2). The corresponding ephemeris for the mid-eclipse timing results to

$$\mathrm{HJD(min)} = 2\,456\,658.64779(74) + 0^{\mathrm{d}}.13952(25)\ \mathrm{E}. \quad (9)$$

The eclipse is comparatively shallow, with a depth of $\sim 0.3^{\mathrm{m}}$. The very small amount of flickering in the light curve and the diminished pre-eclipse hump indicates that DY Pup is a high mass-transfer CV.

3.6 V363 Sgr (1927)

For a long time, the identification of this post-nova was ambiguous. Tappert et al. (2014) found, ~40 arcsec from the published position, a star with a blue continuum and narrow and weak emission lines. They suggest a low orbital inclination, but a rather high accretion rate. No orbital period of this star has been published. This nova was part of our CTIO data set, consisting of typically two subsequent data points per night every three nights over a range of 356 d. A period analysis of that data revealed an unambiguous signal at $f =$ 7.93 c/d that corresponds to a periodic hump or sinusoidal variation with $P = 3.03$ h which we interpret as the orbital period (Fig. 5). The corresponding ephemeris for the maximum is

$$\mathrm{HJD(max)} = 2\,456\,583.579(45) + 0^{\mathrm{d}}.126066(95)\ \mathrm{E}. \quad (10)$$

This value places V363 Sgr inside the period gap of CVs as defined by Knigge (2006). The existence of the photometric modulation indicates a medium-high inclination, somewhat contradicting the conclusion by Tappert et al. (2014) based on the narrow emission lines. However, V363 Sgr could also be a permanent superhumper which allows for lower inclinations (Smak 2010). In this case the orbital period could be a few per cent different from the above value.

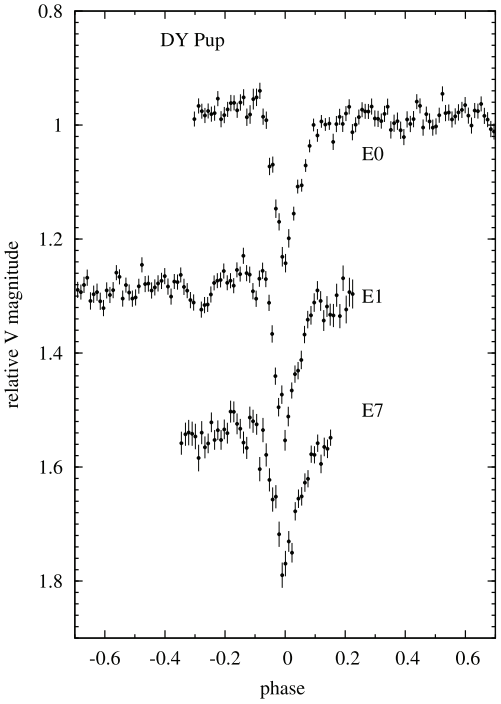

Figure 4. V magnitude versus phase using the ephemeris (9) for DY Pup.

Table 2. Epochs for the eclipsing systems.

Object	E	HJD −2 450 000 d	O–C d
X Cir	−3041	6696.7977	0.0044
	−3028	6698.8051	0.0038
	−2931	6713.7858	0.0020
	−2879	6721.8137	−0.0020
	−2782	6736.7933	−0.0050
	−2058	6848.6214	−0.0056
	−26	7162.4907	0.0020
	−25	7162.6453	0.0021
	−24	7162.8000	0.0023
	−19	7163.5690	−0.0010
	−12	7164.6497	−0.0015
	0	7166.5036	−0.0011
	311	7214.5411	−0.0005
DY Pup	0	6658.6478	0.0001
	1	6658.7873	−0.0001
	7	6659.6245	0.0001

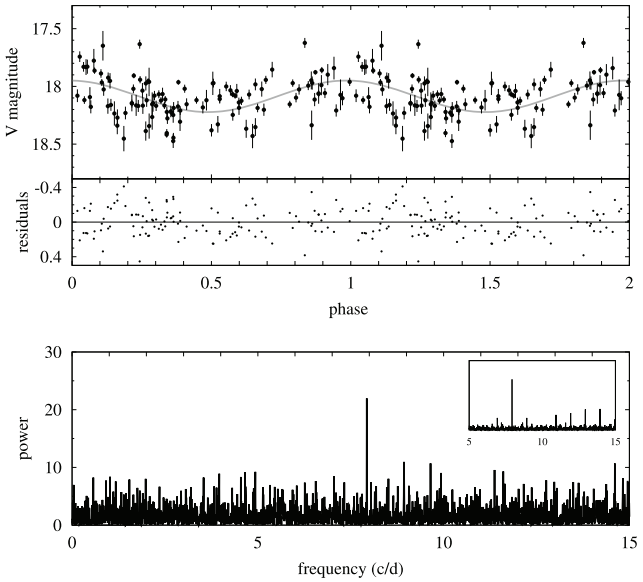

Figure 5. Top: Phased light curve for V363 Sgr according to ephemeris (10) together with a sine fit (grey line). Middle: Residuals of the fit. Bottom: Periodogram showing the highest peak corresponding to $f = 7.93$ c/d. As inset plot the spectral window centred at this frequency is shown.

3.7 V2572 Sgr (1969)

Tappert et al. (2012) give a brief description of the eruption light curve of this object and present a spectrum with comparatively weak Balmer emission lines, the He I series and Bowen/He II. They concluded that V2572 Sgr could be a high mass transfer system. In our attempts to determine its period, the periodogram of our radial velocities measured with EFOSC2 in 2011 showed a strong and broad peak at $f = 7.49(07)$ c/d corresponding to $P_{\rm orb} = 3.20$ h and a broad and predominant alias at $f = 6.45(02)$ c/d (Fig. 6f). One V-band light curve with 3.15 h time span, obtained with the same instrument in 2012 exhibited a hump structure with strong flickering (Fig. A5). If an orbital signature is present, the period should be larger than 3.15 h, because these data clearly do not cover a full orbit, thus frequencies >7.6 c/d can be discarded. The V-band light curves taken at du Pont reveal a periodic hump with a variable amplitude, up to $\sim 0.3^{\rm m}$. The periodogram of this campaign (Fig. 6e) shows a central peak at frequency 6.38(04) c/d and two aliases at 5.35(08) and 7.41(08) c/d of similar height as the central one, being these values comparable to those found in the radial velocities periodogram. Folding the radial velocities and the du Pont photometry according to these frequencies yielded reasonable light and radial velocity curves for the frequencies 6.38 and 7.41, but systematically offsets for individual data sets from the general behaviour for $f = 5.38$ c/d, so that it was discarded.

V2572 Sgr was also included in the CTIO data set, in two seasons, implying a total coverage of nearly one year (see Fig. A3). The search for periodicities was performed independently in each of the two data sets as well as combining all the data to a single set. Its periodograms present large noise level due to the high cadence (only two points per night), however a narrow and outstanding frequency at $f_1 = 6.40(01)$ c/d in each of the single sets and in the combined one is present, together with several frequencies of similar height (Fig. 6d). The frequencies at 6.47(01) and 6.66(01) c/d were discarded because the light curves from du Pont are not fitted properly with these periods. Comparing with the results from the du Pont data, this leaves only two viable frequencies $f_1 = 6.40(01)$ and $f_2 = 7.41(01)$ c/d. Accordingly, we assumed that the orbital frequency could be equivalent to $P_1 =$

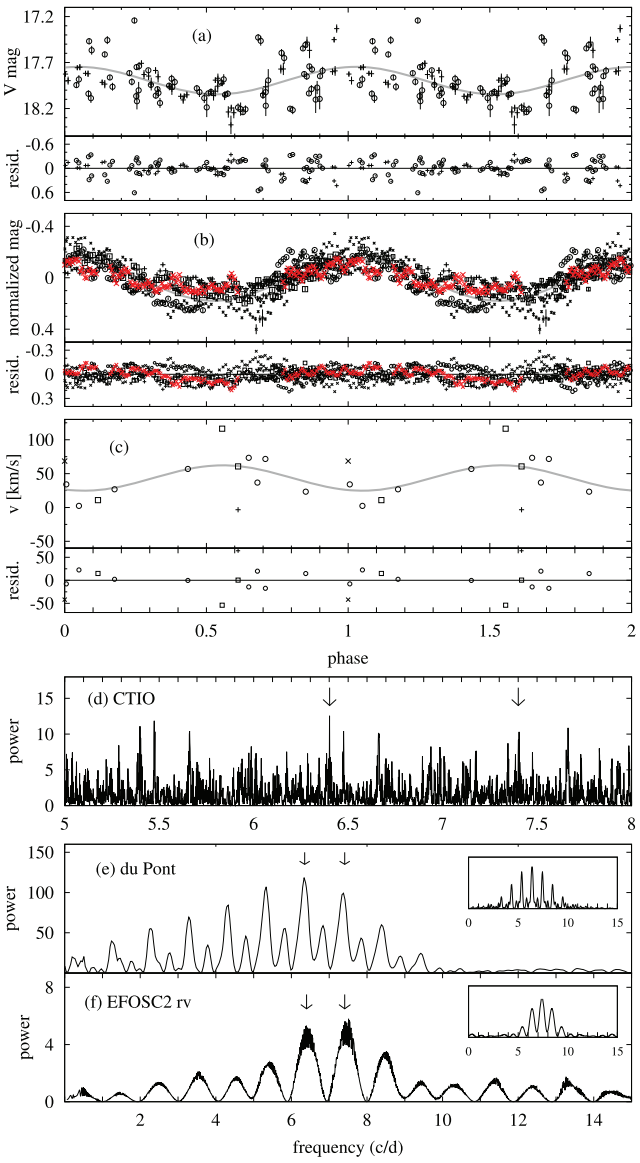

Figure 6. (a): Phase light curves of V2572 Sgr folded with the ephemeris (11) for CTIO data. set 1 and 2 are shown with crosses and circles, respectively. (b) The same for EFOSC2/NTT's light curve (red crosses) and du Pont observations (different black symbols represent different nights). (c) Radial velocity fitted with the ephemeris (11). A sine curve fitted to the data as a grey line and residuals are also shown. Scargle Periodogram for (d) CTIO data in the range of $f = 5 - 8$ c/d. (e) du Pont photometric data (f) radial velocity data. As inset plot is shown the spectral window centred at the dominant frequency. The arrows point to $f = 6.40$ c/d and $f = 7.41$ c/d (see the text for details).

0.156211(29) d or $P_2 = 0.135125(22)$. For both, the rather accurate period allowed us to bridge the CTIO data to those of du Pont enabling us to derive a unique cycle number difference between their epochs and, consequently, also to that of the early EFOSC2 run.

For the final ephemerides we used not only the hump maxima, but also the minima which happen to appear always very near to phase 0.5 in all time-resolved data. Those epochs correspond to the extremes of a polynomial function of degree two fitted for both EFOSC2 and du Pont HJD data. For CTIO data those epochs were derived from the phase data plot. We identified the HJD of the points located close to zero phase and those close to phase 0.5. Making sure that a slight variation of the orbital period did not have a markedly effect

Table 3. Epochs of humps observed in the time-resolved data for V2572 Sgr. The E_1, $(O-C)_1$, and E_2, $(O-C)_2$ values refer to equation (11) and to equation (12), respectively.

HJD −2 450 000 d	E_1	E_2	$(O-C)_1$ (d)	$(O-C)_2$
		EFOSC2		
6063.759(06)	− 2842	− 3285	0.023	− 0.021
6063.829(70)	2841.5	− 3284.5	0.015	− 0.019
		CTIO		
6507.684(25)	0	0	− 0.014	0.028
6510.732(36)	19.5	22.5	− 0.013	0.035
6792.907(50)	1826	2111	− 0.039	0.008
6838.770(30)	2119.5	2450.5	− 0.025	− 0.003
		du Pont		
7162.853(08)	4194	4849	− 0.009	− 0.010
7163.810(02)	4200	4856	0.010	0.001
7163.890(08)	4200.5	4856.5	0.012	0.013
7164.748(01)	4206	4863	0.011	− 0.007
7164.822(01)	4206.5	4863.5	0.007	− 0.001
7164.903(07)	4207	4864	0.010	0.013
7166.765(03)	4219	4878	− 0.003	− 0.017
7214.662(08)	4525.5	5232.5	0.015	− 0.021

on their position in phase space they were then counted as maxima and minima, i.e. the respective HJDs were assigned to full and half cycles, respectively. It should be mentioned that a high uncertainty is associated to this calculation, since those two points per night can correspond to any part of the wide hump. Table 3 gives the resulting cycle numbers E and HJD epochs considering both periods; integer numbers nE refer to observed maxima, the remaining ones to minima. A least square fit through the data nE_1 in Table 3 yields the ephemeris for the hump maximum

$$\mathrm{HJD(max)} = 2\,456\,507.6959(66) + 0^{\mathrm{d}}.1562146(19)\,\mathrm{E}, \quad (11)$$

with a standard deviation of $\sigma = 0.018$ d and for f_2

$$\mathrm{HJD(max)} = 2\,456\,507.6563(66) + 0^{\mathrm{d}}.1351221(16)\,\mathrm{E}, \quad (12)$$

with a standard deviation of $\sigma = 0.018$ d. Phased light curves considering the ephemeris (11), for all photometric data sets are shown in the upper part of Fig. 6. The sinusoidal parameters for the radial velocities listed in the supplementary online material, according to P_1 are $\gamma = 44(7)\,\mathrm{km\,s^{-1}}$ and $K = 19(8)\,\mathrm{km\,s^{-1}}$ and for P_2 are $\gamma = 47(5)\,\mathrm{km\,s^{-1}}$ and $K = 26(8)\,\mathrm{km\,s^{-1}}$.

3.8 XX Tau (1927)

The history of this nova that erupted in 1927 has been extensively described by Schmidtobreick et al. (2005) who also present an optical spectrum dominated by strong Balmer and He I emission lines resembling more a dwarf nova than an old nova. However, the CTIO data did not present any clear evidence for outburst behaviour in roughly 1.5 yr spanning monitoring.

Rodríguez-Gil & Torres (2005) found a number of periodicities in time-series photometric data at periods of 23.69(03) min, 3.26(05) h, and 5 d. While the shortest value was considered as very uncertain, the middle one was attributed to an orbital or superhump modulation, and the longest period was interpreted as evidence of an eccentric/tilted accretion disc.

Our light curves taken in a five nights spanning observing run at the 2.5-m du Pont are dominated by strong irregular flickering. The periodogram does not show any sign of the suspected orbital or

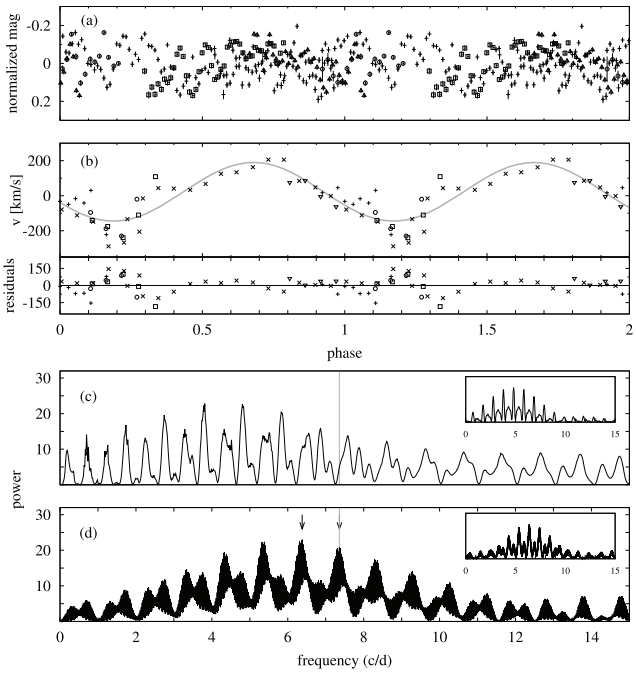

Figure 7. (a) Photometric phased light curve for XX Tau according to ephemeris (14). (b) Radial velocity, the sine fit, and the residuals. Different nights are shown as different symbols. Phases very likely do no coincide because two data sets have different T_0. (c) Periodogram of the photometric data together with the spectral window centred at the main frequency. The vertical grey line indicates the position of the detection made by Rodríguez-Gil & Torres (2005). (d) Periodogram of the radial velocities. The arrows point to the frequencies f_1 and f_3 (see the text for details).

superhump modulation (Fig. 7c). Instead, its highest peak is at $f = 4.82(06)$ c/d, equivalent to $P = 4.98$ h. However, this signal is clearly not stable (Fig. A6), and thus probably is simply caused by flickering mimicking a periodicity within our comparatively short time-series.

Radial velocities measured from time-series spectroscopic data taken at FORS2/VLT in five nights spanning two weeks in total show a periodogram with a central peak and a number of significant broader one-day aliases, each one composed of a number of narrow peaks as can be seen in bottom panel of Fig 7. The broad central peak is at $f_1 = 6.38(01)$ c/d (equivalent to 3.76 h), the second most significant at $f_2 = 5.38(06)$ c/d (4.46 h), the third at $f_3 = 7.36(01)$ c/d (3.26 h) and others at $f_4 = 4.31(06)$ c/d (5.57 h), $f_5 = 8.29(06)$ c/d (2.90 h) and $f_6 = 9.29(01)$ c/d (2.58 h). We noted that f_3 agrees well with the period favoured by Rodríguez-Gil & Torres (2005). However, the periodogram presented in that article (their fig. 14) shows a number of similarly strong aliases that are not properly discussed by the authors. A comparison with the periodogram for our data shows that all our significant frequencies coincide with the peaks in their periodogram. Thus, we find that, from the periodograms, we have six valid frequencies. However, folding our data with each of the corresponding periods for frequencies f_2, f_4, f_5 and f_6 showed systematic deviations from the fit (e.g. in the sense that a data set from one specific night presented a systematic offset), while for f_1 and f_3 the distribution of all data was consistent with random noise. As mentioned above, each broad peak in our periodogram is formed by a series of narrow peaks, and thus each of the broad peaks for f_1 and f_3 contains several valid frequencies, which are displayed in Table 4. We thus here give the respective strongest ones of those as fiducial frequencies, but have to keep in mind that more valid

Table 4. Values of the possible orbital frequencies and its respective orbital period for XX Tau within one FWHM of the broad peaks centred at $f_1 = 6.38$ c/d and $f_3 = 7.36$ c/d in the periodogram shown in Fig. 7 (d).

f c/d	P d	f c/d	P d
f_1		6.48(02)	0.15432(45)
6.14(01)	0.16289(30)	6.51(02)	0.15364(45)
6.16(01)	0.16223(30)	f_3	
6.19(01)	0.16158(30)	7.19(01)	0.13908(22)
6.21(01)	0.16093(29)	7.21(01)	0.13863(22)
6.24(01)	0.16033(29)	7.24(01)	0.13816(22)
6.26(01)	0.15971(29)	7.26(01)	0.13768(22)
6.29(01)	0.15904(29)	7.29(01)	0.13724(21)
6.31(01)	0.15848(29)	7.31(01)	0.13678(21)
6.34(01)	0.15782(28)	7.34(01)	0.13632(21)
6.36(01)	0.15724(28)	7.38(01)	0.13544(21)
6.41(01)	0.15609(28)	7.41(01)	0.13499(21)
6.43(01)	0.15546(28)	7.43(01)	0.13452(21)
6.46(01)	0.15485(27)	7.46(01)	0.13408(20)

possibilities within $3\sigma \sim 0.2$ c/d exist. Defining T_0 as the red-to-blue crossing time in the radial velocities sinusoidal fit, the ephemeris for f_1 then is

$$\mathrm{HJD} = 2\,458\,484.620(23) + 0^{\mathrm{d}}.0.15664(28)\ \mathrm{E}, \quad (13)$$

and for f_3 is

$$\mathrm{HJD} = 2\,458\,484.632(45) + 0^{\mathrm{d}}.13588(21)\ \mathrm{E}. \quad (14)$$

As example, in Fig. 7 we show the light curve and the radial velocities folded with the period from equation (14), since this is the value favoured by Rodríguez-Gil & Torres (2005). The sinusoidal fit corresponding to this period exposes a wide semi-amplitude $K = 167(12)\,\mathrm{km\,s^{-1}}$ and the systemic velocity $\gamma = -22(10)\,\mathrm{km\,s^{-1}}$ is slightly blueshifted. In the case for f_1 the fit parameters are $K = 160(16)\,\mathrm{km\,s^{-1}}$ and $\gamma = -10(8)\,\mathrm{km\,s^{-1}}$. The photometric data (Fig. 7 top) does not show any modulation for either period.

One possibility for the modulation found (Rodríguez-Gil & Torres 2005) not being present in our photometric data is that strong flickering on larger time-scales than in the LCO data mimicked a periodic signal in their data. However, this flickering would then have maintained these same properties over a time span of six nights, which appears unlikely. Furthermore, the proximity to the spectroscopic signal is suspicious. A different possibility is that the system was caught in two different brightness states. In that case, the data from Rodríguez-Gil & Torres (2005) could correspond to a state with a fainter accretion disc, where the bright-spot would be more dominant and thus could produce an orbital hump in the light curve. In brighter, optically thick, accretion discs, on the other hand, the bright-spot is typically much diminished or even not visible at all (Warner 2003a). Still, the long-term light curve from Vogt et al. (2018), if noisy, is consistent with a constant brightness over a range of about 1.5 yr. However, comparing our spectroscopic data with that of Schmidtobreick et al. (2005), we find that the equivalent width of the Hα line in our data with 28 Å amounts to only roughly half the value that they found in their data (52 Å). This points to a difference in the disc brightness, with a stronger line indicating a fainter disc. Unfortunately, we do not have any calibrated photometric information for either the Schmidtobreick et al. (2005) nor the Rodríguez-Gil & Torres (2005) data. However, reviewing above evidence and sorting the dates, we find that XX Tau likely inhabited

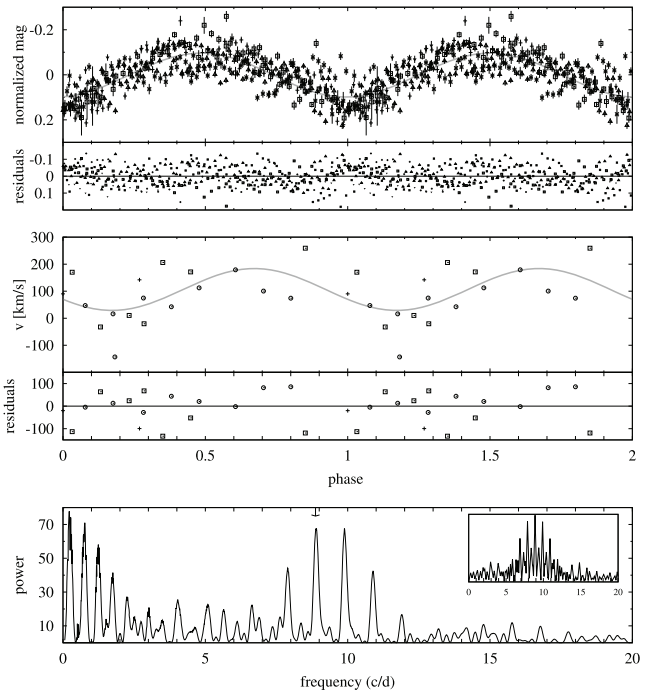

Figure 8. Top: Phased light curve for CQ Vel according to ephemeris (15), the sinus fit to the orbital modulation (grey line) and the residuals of the sine fit are shown. Middle: Radial velocity, the sinus fit, and the residuals. Bottom: Periodogram of the photometric data including its spectral window centred to frequency pointed with the arrow.

a fainter disc in late 2002 October and early November (Rodríguez-Gil & Torres 2005), and in 2003 January (Schmidtobreick et al. 2005), but a brighter disc in 2013 December and 2014 January (our photometric data) and in 2018 December and 2019 January (the spectroscopic data). The long-term CTIO data covers the range from 2013 November to 2015 April. This timeline is thus consistent with the possibility that XX Tau at some point between 2003 January and 2013 November (at least once) underwent a change from a low mass-transfer state with a faint disc to a higher mass-transfer state with a brighter one.

3.9 CQ Vel (1940)

This nova reached its maximum brightness, $m_{\mathrm{pg}} = 9^{\mathrm{m}}$ in 1940 April 19, being discovered on Franklin-Adams plates by C. J. Van Houten (Hoffleit 1950). It was categorized as a moderately fast nova with $t_3 = 53$ d (Duerbeck 1981) and a large amplitude ($\mathrm{A}_v > 13.1^{\mathrm{m}}$). The nova was recovered by Woudt & Warner (2001), who performed high speed photometry in the field of a candidate for the nova proposed by Duerbeck (1987). A strong flickering activity in a single, 4.07 h long, light curve was detected in an object 9 arcsec from the suspected position. Spectroscopic observations made by Schmidtobreick et al. (2005) using those coordinates confirmed the post-nova. They reported an equivalent width of Hα line as 18 Å, while from our new EFOSC2 spectra the value is 14.5 Å.

Our light curves (Fig. A7) show strong flickering activity as was seen by Woudt & Warner (2001). The periodogram of the photometry (Fig. 8) shows two dominant frequencies at $f_1 = 8.87$ and $f_2 = 9.86$ c/d. Using both frequencies, we found the following ephemerides for the photometric minima

$$\mathrm{HJD(min)} = 2\,456\,655.786(03) + 0^{\mathrm{d}}.11272(12)\ \mathrm{E}, \quad (15)$$

for f_1 and the alternative:

$$\mathrm{HJD(min)} = 2\,456\,655.782(06) + 0^{\mathrm{d}}.0.10138(24)\ \mathrm{E}. \quad (16)$$

The RMS scatter of the observed minima around ephemeris (15) is 0.0039 d and for (16) is 0.0088 d. Both the radial velocity and the photometric data were folded with these ephemeris, however no significant differences were found. In the same way, the average semi-amplitude (K) for the photometric phased data are practically identical within the errors, $K = 0.0966(32)$ mag and $K = 0.0932(34)$ mag, respectively.

We also note that, while a photometric sinusoidal signal could in principle be explained as the result of ellipsoidal modulation with orbital period twice the observed period, the radial velocities from our EFOSC2 spectra rule this out. The sine fit according to equation (15) yields a systemic velocity $\gamma = -106(15)\,\mathrm{km\,s^{-1}}$ and a semi-amplitude $K = 77(20)\,\mathrm{km\,s^{-1}}$.

Under those circumstances, a decision regarding which of the alternatives is the correct one must await more data. In any case, both of these periods place CQ Vel within the period gap.

3.10 RW UMi (1956)

In the Ritter & Kolb (2003b) catalogue, RW UMi is listed as the nova with the shortest orbital period that is not marked as 'uncertain'. The value of $P = 0.05912(15)$ d is based on photometric data taken in 14 nights over a total time range spanning almost four months (Retter & Lipkin 2001). The period corresponds to a sinusoidal variation in the light curve with an amplitude of 0.05^{m} in white light. Later photometric studies by Bianchini et al. (2003) and Tamburini et al. (2007) found a number of other periodicities with larger amplitudes, suggesting that RW UMi is an intermediate polar showing quasi-periodic oscillations. They also found that the brightness of the nova is still declining at an approximate rate of $0.03\,\mathrm{mag\,yr^{-1}}$ as measured from the year 1988 to 2006. The existence of multiple photometric periods lets the identification of the reported value with an orbital modulation appear ambiguous, thus motivating the present spectroscopic study.

Compared to other post-novae, the emission lines in RW UMi are relatively strong, with Hα presenting an equivalent width of -17 Å. However, the line profile is complex and non-Gaussian, with a broad base and a more narrow main component, with likely more than one source contributing to the latter, as evidenced by its markedly variable shape (Fig. A1). Additionally, we were unfortunate in that the longest data set counted with the worst weather conditions of the three nights, resulting in significantly diminished S/N. Finally, obtaining a conclusive radial velocity curve is further complicated by the line presenting a comparatively small Doppler shift. In view of these difficulties, we employed a number of methods to determine the radial velocities, measuring different parts of the line or using the manual cross-correlation mentioned above. However, we found that in the end the clearest curve was produced by fitting a single Gaussian function to the full line profile. The corresponding Scargle periodogram is presented in Fig. 9. The strongest peak corresponds to a frequency $f = 16.80(10)$ c/d, with the uncertainty being estimated by assuming a normal distribution. This translates to a period $P = 0.0595(4)$ d, which, within one sigma, is identical to the photometric period of Retter & Lipkin (2001). Our periodogram shows several aliases that are close in strength to the main peak, and, taken on its own, it does not represent sufficient evidence to assign the orbital period. However, the good agreement with the photometric period strongly suggests that this indeed reflects the orbital motion of the system.

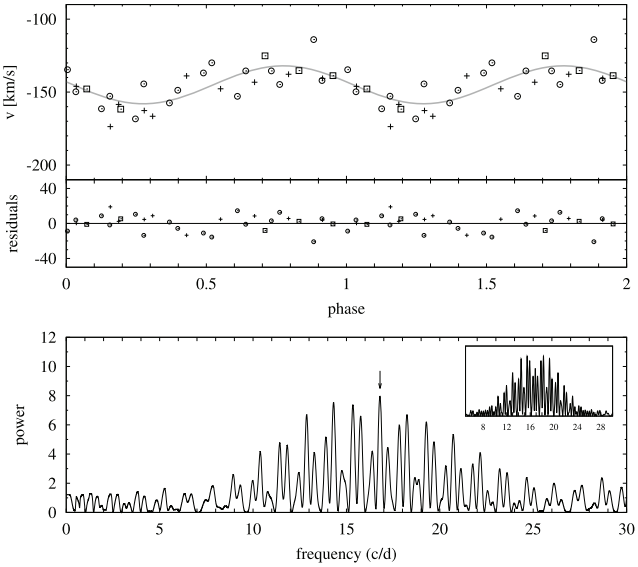

Figure 9. Top: Phase-folded radial velocities of RW UMi, the corresponding sine fit according to equation (17) and the residuals. Different symbols indicate data from different nights. Bottom: Scargle periodogram of the radial velocity data. The arrow marks the highest peak at $f = 16.80(10)$ c/d. As inset plot is shown the spectral window centred at this frequency.

Table 5. Ephemerides for the eclipsing systems whose orbital periods could be confirmed by the CTIO observations (Vogt et al. 2018). T_0 refers to minima of eclipses.

Name	T_0 HJD − 2 400 000	P_{orb} d
OY Ara	56516.5722(10)	0.155390(30)
V849 Oph	48799.7412(18)	0.17275611(06)
WY Sge	47059.8678(04)	0.153634547(10)
V728 Sco	56015.8066(09)	0.13833866(18)

A sine fit to the radial velocity data according to equation (1) yields the aforementioned small semi-amplitude $K = 13(1)\,\mathrm{km\,s^{-1}}$ and a markedly blueshifted systemic velocity $\gamma = -145(1)\,\mathrm{km\,s^{-1}}$ (lower plot in Fig. 9). Choosing the red-to-blue crossing of the radial velocities as the zero-point of the phase-folded curve and using the more precise photometric period yields a formal ephemeris of

$$\mathrm{HJD} = 2\,457\,196.4397(10) + 0^{\mathrm{d}}.059\,12(15)\ \mathrm{E}\ , \quad (17)$$

although, considering the complex nature of the line profile, it is unlikely to correspond to the superior conjunction of the white dwarf.

3.11 Improved ephemerides of eclipsing novae with previously known orbital periods

We present refined orbital periods of WY Sge, V728 Sco, OY Ara, and V849 Oph from CTIO data, which, by chance, have occasionally been caught during eclipse phases, showing fainter brightness than normally. The resulting ephemerides are listed in Table 5. Their epochs and O–C values, together with previously available literature and their references are listed in Table A6. Because the CTIO data consist of only two data points in any given night, they do not necessarily correspond to the central part of and eclipse, and thus the corresponding O–C deviations are larger in average than those from published photometry. Despite this, due to the larger time intervals covered now the new periods are more accurate.

We also have performed searches for periodicity in the other novae included in the CTIO data, V500 Aql, HS Pup, V1059 Sgr, and V373 Sct, without finding any significant photometric periodicity.

4 THE ORBITAL PERIOD DISTRIBUTION OF NOVAE

The current sample analysed here contains 92 orbital periods. From the sample listed by Tappert et al. (2013), we selected those periods that satisfied the criteria defined below, giving a total of 74 periods, to which six new periods presented here were added, together with those new periods listed by Ritter & Kolb (2003b) (version 7.24, 2016) since 2013.

Here we present an analysis of the observed orbital period distribution of novae and compare it to simulated distributions both from the literature and with a newly established one that takes into account consequential angular momentum loss.

4.1 Observed period distribution

We used the catalogue of Ritter & Kolb (2003a; version 7.24, 2016) to gather the period information on the novae included here. We excluded objects from the sample if their tabulated periods: (a) were not sufficiently coherent and might be attributed to QPOs; (b) might be caused by ellipsoidal variations at twice the orbital period; and (c) were based on data that has never been published. In addition, we (d) excluded objects for which the CV classification is not confirmed, with the data allowing for alternatives (e.g. in the case of light curves showing comparatively smooth sinusoidal variations that could also originate in pulsating stars). Table 6 presents the 24 novae that were excluded from the sample based on above criteria. To the such established distribution we added our own results presented in the previous section. We have also included the novae RS Car, IL Nor, V2572 Sgr, XX Tau and CQ Vel, in spite of the fact that in those systems we cannot distinguish between more than one possible values for the orbital period. However, the periods are sufficiently close to correspond to the same period bin in the histogram, so that the overall distribution is identical for either of the alternatives. These novae are marked as 'provisionals' in the Table used (A7) for resulting distribution presented in Fig. 10.

Comparing the current distribution with the one published by Tappert et al. (2013) (in Fig. 10 are shown as a solid black line and grey blocks, respectively) and using their same criteria to analyse the sample , i.e. considering the period gap as the range between 2.15 and 3.18 h (Knigge 2006), it is evident that both follow the same trend, with a strong maximum in the range of 3–4 h. In the new distribution most of the periods are above the period gap, corresponding to 79 per cent (equivalent to 72 objects), out of which 45 systems have $P_{\rm orb} > 4$ h, equivalent to ∼50 per cent of the total sample. The peak in the 3–4 h period range becomes more pronounced, concentrating 34 percent of the total sample (equivalent to 31 novae). On the other hand, eight per cent of the post-novae, corresponding to seven systems, are below the period gap and 14 per cent are in the period gap (corresponding to 13 systems).

Table 6. Novae with uncertain published $P_{\rm orb}$. The last column indicates the exclusion criterion as defined in the text.

Name	$P_{\rm orb}$ (h)	Outburst	Ref.	Cause
V705 Cas	5.47	1993	(1)	(c)
V842 Cen	3.94	1986	(2)	(a)
V2274 Cyg	7.2	2001	(3)	(c)
V2362 Cyg	1.58	2006	(4)	(c)
V2491 Cyg	17	2008	(5)	(a)
DM Gem	2.95	1903	(7)	(a)
DI Lac	13.05	1910	(8)	(c)
DK Lac	3.11	1950	(9)	(a)
U Leo	3.21	1855	(10)	(d)
GI Mon	>4.8	1918	(6), (7)	(a)
LZ Mus	4.06	1998	(11)	(c)
V400 Per	3.84	1974	(7)	(a)
V445 Pup	15.62	2000	(12)	(a)
V574 Pup	1.13	2004	(13)	(b)
V1186 Sco	1.39	2004	(3)	(c)
V1324 Sco	3.8	2012	(14)	(c)
V726 Sgr	19.75	1936	(15)	(d)
V999 Sgr	3.64	1910	(15)	(b)
V1174 Sgr	7.42	1952	(15)	(d)
V4077 Sgr	3.84	1982	(16)	(c)
V5582 Sgr	3.76	2009	(15)	(b)
V5980 Sgr	30.34	2010	(15)	(b)
V382 Vel	3.79	1999	(17), (18), (19)	(a)
PW Vul	5.13	1984	(20)	(c)

Note. References: (1) Retter & Leibowitz (1995), (2) Woudt et al. (2009), (3) Ritter & Kolb (2003a), (4) Balman, Nasiroglu & Akyuz (2009), (5) Zemko et al. (2018), (6) Woudt, Warner & Pretorius (2004), (7) Rodríguez-Gil & Torres (2005), (8) Goransky et al. (1997), (9) Katysheva & Shugarov (2007), Honeycutt et al. (2011a), (10) Downes & Szkody (1989), (11) Retter, Liller & Garradd (1999b), (12) Goranskij et al. (2010), (13) Walter et al. (2012), (14) Finzell et al. (2018), (15) Mróz et al. (2015), (16) Diaz & Bruch (1997), (17) Woudt, Warner & Spark (2005), (18) Balman, Retter & Bos (2006), (19) Egan et al. (2014), (20) Hacke (1987)

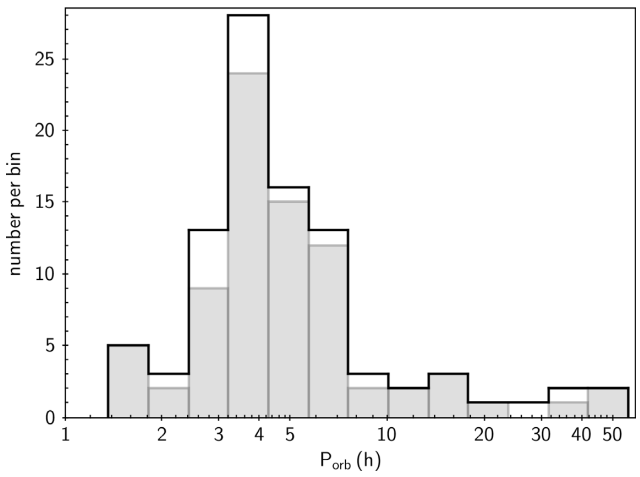

Figure 10. The current orbital period distribution of the novae on logarithmic scale (solid black line) in comparison with the distribution published previously by Tappert et al. (2013, grey blocks).

4.2 Simulation

We generated an initial main-sequence plus main-sequence (MS+MS) binary population of 10^9 systems with the following assumptions: initial-mass function of Kroupa, Tout & Gilmore (1993) for the mass of the primary star; flat initial mass-ratio distribution for the mass of the secondary star (Sana, Gosset & Evans 2009); distribution of initial orbital separations (a) flat in log a ranging from $a = 3$ to $10^4 R_\odot$ (Popova, Tutukov & Yungelson 1982; Kouwenhoven et al. 2009); constant star formation rate within the age of the Galaxy (13.5×10^9 yr; Pasquini et al. 2004); solar metallicity; and no eccentricity.

The binary-star evolution code (BSE) from Hurley, Tout & Pols (2002) was used to evolve the systems until the end of the common-envelope phase, i.e. until the close but detached WD+MS binaries (which are the direct progenitors of CVs) are formed. A common-envelope efficiency of $\alpha_{\rm CE} = 0.25$ was assumed (Zorotovic et al. 2010) and the binding energy parameter λ was computed assuming that the recombination energy stored in the envelope does not contribute to the ejection process (Zorotovic, Schreiber & Parsons 2014). After this phase, the WD+MS systems were evolved using the CV evolution code developed by us and described in Schreiber, Zorotovic & Wijnen (2016) and Zorotovic et al. (2016). It is based on the disrupted magnetic braking model for systemic angular momentum loss (AML), i.e. AML that is present even in the absence of mass transfer, due to gravitational radiation and magnetic wind braking (the latter only for CVs above the period gap). Inflation of the radius of the secondary star as a consequence of mass transfer is incorporated by using the observed mass–radius relation and the scaling factors for systemic AML from Knigge et al. (2011). This code also takes into account the consequential AML produced by mass transfer and nova eruptions after the CV phase begins. Two models for consequential AML due to nova eruptions were included: the classical non-conservative model from King & Kolb (1995) and the empirical model from Schreiber et al. (2016). The latter predicts a smaller number of CVs, mainly because systems with low-mass WDs are driven into a dynamically unstable mass transfer regime and merge. As shown in Schreiber et al. (2016), this has an effect not only on the WD mass distribution but also on the distribution of orbital periods. Here we want to test if there is also an effect on the predicted orbital period distribution of post-nova systems.

Once the simulated populations of CVs have been generated, the probability of observing a nova eruption was computed for each system. This probability is inversely proportional to the nova recurrence time $P_{\rm rec}$, which can be written as

$$P_{\rm rec} = m_{\rm acc}/\dot{M}, \tag{18}$$

where $\dot{M}$ is the mass transfer rate and $m_{\rm acc}$ is the accreted mass needed to produce a nova outburst. For each system we derived the value for $m_{\rm acc}$, which depends on the WD mass, the mass transfer rate, and the core temperature, based on Yaron et al. (2005, interpolating their table 2), who presented models for different fixed core temperatures. Townsley & Bildsten (2004) found that the equilibrium core temperatures of WDs are below 10^7 K in typical CVs, and Chen et al. (2016) compared the observational data of novae in the M31 galaxy with the models from Yaron et al. (2005) and preferred the low temperature models. We have therefore chosen the values of $m_{\rm acc}$ listed by Yaron et al. (2005) for their models with the minimum core temperature (10^7 K).

We also defined systems that experience more than a nova eruption in a century as recurrent novae (e.g. Shara et al. 2018). This means that if the computed recurrence period of a system in our simulation is less than 100 yr, more than one nova eruption could be observed during that period of time. Therefore, we set an upper limit for the detection probability $\mathcal{P}_{\rm det} = (P_{\rm rec}[{\rm yr}])^{-1}$ of 0.01, which corresponds to a recurrence period of 100 yr, to avoid counting recurrent novae more than once in the simulated period distribution.

Systems in which the mass of the donor star falls below $0.05 M_\odot$ were eliminated from our simulated sample, because their mass–radius relation is not well constrained (e.g. Knigge et al. 2011). This has virtually no effect on the simulated distribution of orbital periods, because CVs with low-mass donors (below the brown-dwarf mass limit) have very low mass transfer rates which translate into very long recurrence periods, i.e. extremely low probabilities of being detected as post-nova systems. We also excluded CVs that experienced a thermal time-scale mass transfer phase, i.e. systems with initially massive donors ($M_2 \gtrsim 1.5 M_\odot$), because the evolution during this phase is not well understood (e.g. Nomoto, Nariai & Sugimoto 1979; Hachisu, Kato & Nomoto 1996), and it is especially not clear how the mass of the WD could be affected. However, these systems should make up a small percentage of the current CV population (∼5 per cent; Pala et al. 2020).

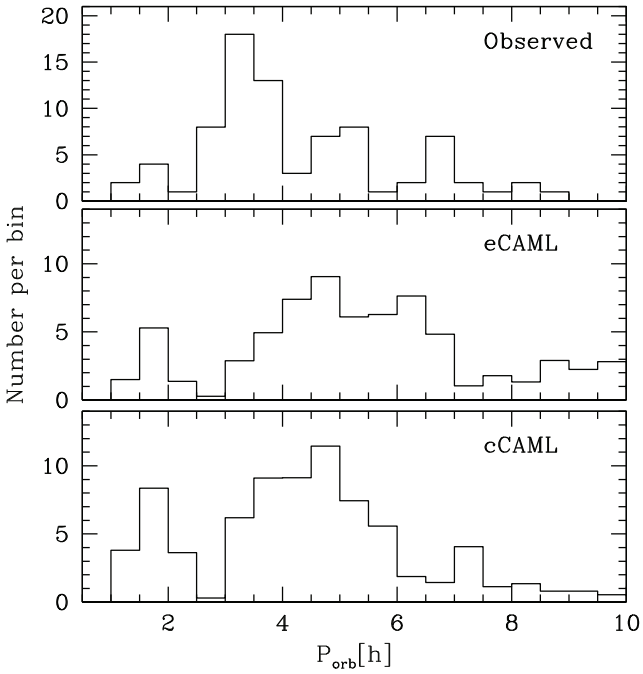

Figure 11. Orbital period distribution of post-nova systems. From top to bottom: observed systems (this work), simulation assuming the empirical consequential AML model from Schreiber et al. (2016) and simulation assuming the classical consequential AML model from King & Kolb (1995).

4.3 Comparison

The predicted orbital period distributions were constructed using the same bins as for the observed distribution, adding the detection probabilities for all the simulated systems within that period range, and normalizing to the observed number of systems. The results are shown in Fig. 11 . The two models of AML predict broadly similar distributions, and both show the majority of systems above the gap, in keeping with the observed distribution (top panel). The classical non-conservative model from King & Kolb (1995, bottom panel) predicts that ∼18 per cent of novae should be observed below the orbital period gap, ∼2 − 3 per cent in the gap, and ∼79 − 80 per cent above it. For the simulations that assume the empirical model from Schreiber et al. (2016, middle panel), the expected fractions are ∼9 − 10 per cent below the gap, only ∼1 per cent in, and ∼89 − 90 per cent above. The empirical model is therefore in better agreement with the observations, regarding the fraction of systems that we expect to observe below the orbital period gap. However, this conclusion should be taken with caution because we are dealing with low-number statistics and our poor knowledge of CV evolution.

The overprediction of systems below the gap in the two simulations with respect to the observed distribution might be explained by poor constrained aspects of CV evolution. A key parameter that might affect the simulated distribution is the assumed core temperature.

As explained before, we used a constant core-temperature for the calculations of the accreted mass needed to produce a nova outburst ($m_{\rm acc}$). As calculated by Yaron et al. (2005), colder WDs should need to accrete more mass before triggering the eruption of a nova. Given that the evolution of a CV towards shorter periods is mainly driven by systemic AML, the lifetime of a system is much shorter above the gap than below it due to the efficiency of magnetic braking. This implies that CVs below the gap are, on average, older than CVs above the gap. Therefore, the core temperature of the WDs in CVs below the gap should be lower, on average, because they have had more time to cool. Also, it is not clear whether the accretion process can affect the temperature of the core of the WD (e.g. Cumming 2002; Townsley & Bildsten 2004; Townsley & Gänsicke 2009). If the core temperature can increase as a result of mass accretion, this increase should be larger for CVs above the gap, in which the accretion rate is higher. Combining these two effects implies that by assuming a constant WD core temperature for all the systems we are probably underestimating the value of $m_{\rm acc}$ needed to trigger a nova eruption for CVs below the gap, which means that their contribution to the predicted post-nova population is overestimated. A more accurate derivation of $m_{\rm acc}$ that depends on the core temperature for each WD is beyond the scope of this paper, but the effect of such an improvement on the models would probably be to reduce the fraction of novae predicted below the gap, for both models.

Another discrepancy with the observations is that our simulations predict an extremely low fraction of novae in the orbital period range that corresponds to the period gap, for both models of consequential AML (below 3 per cent, while observationally it is $\sim$14 per cent). This is a direct consequence of assuming efficient magnetic braking for all CVs above the period gap. However, magnetic braking can become very inefficient for CVs containing WDs with strong magnetic fields. According to Belloni et al. (2020), the WD magnetic field in strongly magnetized CVs can trap part of the wind from the donor reducing the loss of angular momentum through this wind. This implies that magnetic CVs above the gap have lower mass transfer rates than their non-magnetic counterparts, and have therefore less bloated donors. This translates into a shift of the upper edge of the gap towards shorter periods, or even a complete absence of the detached phase for CVs with the strongest WD magnetic fields. In other words, magnetic CVs can cross, or at least enter, the orbital period gap. Indeed, the gap seems to be much less pronounced in the observed period distribution of magnetic CVs than in that of non-magnetic CVs (e.g. Ferrario, de Martino & Gänsicke 2015, their fig. 17). The fraction of magnetic WDs in CVs is known to be high (e.g. $\sim$33 $\pm$ 7 per cent in the first volume-limited sample of CVs, recently published by Pala et al. 2020). Therefore, including a fraction of magnetic CVs in our simulation, with reduced magnetic braking model like the one described by Belloni et al. (2020), could help reconcile the fraction of novae observed in the gap.

Regardless of the model, the main difference between our simulations and the observed period distribution is the presence of a peak in the number of observed systems with periods between 3 and 4 h that our models do not reproduce. Above the period gap, the mass transfer rate depends mainly on the formalism assumed for magnetic braking. Here we assumed the Rappaport, Verbunt & Joss (1983) prescription for $\gamma = 3$, with the normalization factor derived by Knigge et al. (2011). As can be seen in Knigge et al. (2011; their fig. 2), this formulation predicts a reduction in AML when approaching the period gap from larger periods. The simulated mass transfer rates are therefore lower for systems in the period range of $3-4$ h compared to systems with larger periods, making their recurrence periods longer. Knigge et al. (2011) also showed that assuming a smaller value for γ in the Rappaport et al. (1983) prescription for magnetic braking, or the formulation developed by Kawaler (1988, which is the same as the Andronov, Pinsonneault & Sills (2003) model in the unsaturated limit), would all predict an increase of AML towards shorter periods, which would transfer into larger mass transfer rates and smaller recurrence periods that could reconcile the predictions with the observations.

The existence of a peak in the period distribution of post-nova system at $3-4$ h, in addition to observational evidence of higher mass transfer rates for CVs in the same period range (Townsley & Gänsicke 2009; Pala et al. 2017), seems to indicate that the Rappaport et al. (1983) prescription with $\gamma = 3$ might not be the best approximation for magnetic braking in non-magnetic CVs. A similar conclusion is drawn in Belloni et al. (2020), where the simulated mass transfer rates for non-magnetic CVs above the gap drastically disagree from observations (when assuming also $\gamma = 3$ in the Rappaport et al. (1983) prescription for magnetic braking), suggesting that AML caused by magnetic braking is not well understood. An interesting future work would be to derive the normalization factors, similar to what was done in Knigge et al. (2011), but for magnetic braking prescriptions that predict an increase of AML while approaching the gap from larger periods. This would allow us to test whether the peak in the observed period distribution can be reproduced by changing the formulation for magnetic braking only.

Comparing with the literature, the only theoretical orbital period distribution of novae previously published is that of Townsley & Bildsten (2005). They predict a strong peak in the range of $P_{\rm orb}$ = 3–4 h, but their cumulative distributions do not fit well for periods larger than 4 h, which corresponds to $\sim$50 per cent of the observed sample. As the same authors mentioned, they use a very simple CV population model, where the number of CVs at each period interval was taken from Howell, Nelson & Rappaport (2001) with a fixed WD mass, instead of evolving the systems from a binary population synthesis model. In order to obtain the mass transfer rate, they used the same prescription as we did for magnetic braking (i.e. Rappaport et al. 1983 prescription with $\gamma = 3$), but with a different mass–radius relation for the donor stars above the gap (also from Howell et al. 2001). The accreted mass needed to produce a nova outburst was based on Townsley & Bildsten (2004) instead of Yaron et al. (2005). It is therefore impossible to make a more detailed comparison between their models and ours, although the need to include magnetic CVs with reduced magnetic braking in order to reproduce the fraction of novae observed in the period gap is a common conclusion of both studies.

5 SUMMARY AND CONCLUSIONS

We have presented six new orbital periods and have reviewed and/or improved the periods for eight old novae, and discussed the resulting distribution of observed orbital periods with respect to theoretical predictions based on a binary population synthesis model. In the following, we summarize the most noteworthy results and conclusions.

(i) With X Cir, we report one new eclipsing nova, and with DY Pup, we confirm another one that was previously reported, but lacked the data to sustain such claim. Both have orbital periods in the $3-4$ h range, corresponding to the period regime that is dominated by high $\dot{M}$ objects. Comparing those systems, we find that the eclipses in DY Pup with a depth of $\sim 0.3^{\rm m}$ are considerably more shallow than those of X Cir that show an average depth of $1^{\rm m}$, which could indicate that the latter object is seen at a somewhat higher inclination than the

former. X Cir's high inclination could also possibly account for the spectral appearance that was interpreted by Tappert et al. (2014) as a signature of a low $\dot{M}$ system (Warner 1986).

(ii) For RS Car, IL Nor, V2572 Sgr, XX Tau, and CQ Vel, there is still some ambiguity concerning the orbital period, with more than one possible values existing for both objects. Still, we can already conclude that CQ Vel, together with V363 Sgr are situated in the period gap, while IL Nor is placed below it, making it the oldest nova in that short-period regime. The detection of an orbital modulation in the light curve of V363 Sgr indicates that it is seen at a somewhat higher inclination than suspected by Tappert et al. (2014).

(iii) For three targets (V2572 Sgr, CQ Vel, and RW UMi) the orbital period was determined or confirmed by time-resolved radial velocity observations. For the confirmation of the orbital period for XX Tau, we suggest trying by this technique observing with a baseline larger than 4 h.

(iv) In addition to short-term time-resolved photometric observations, we also used the CTIO data set, with a typical time resolution of 3–4 d, a by-product of a search for stunted dwarf nova-like outbursts in classical novae (Vogt et al. 2018). Our new period of V363 Sgr is entirely based on these data; they also enabled us to derive a long-term orbital ephemeris of V2572 Sgr, and to improve the periods of other six novae (four with eclipses and two with orbital humps).

(v) We also present a statistic of all currently known orbital periods of novae, which are distributed in the following way: 79 per cent are located above the gap, equivalent to 72 objects, ∼50 per cent of them (= 45 objects) have $P_{\rm orb} > 4$ h. Only seven systems are located below the period gap, corresponding to eight per cent of the sample, meanwhile 13 systems (14 per cent) were found within the period gap. It is worth mentioning here again that this distribution differs significantly from the one of all CVs, with the main differences being the low number of objects below the gap, the majority of the novae having period above the gap, and especially the peak located above the gap at 3–4 h that with the new data has become even more pronounced.

(vi) There are striking differences between the theoretically predicted period distribution of novae and the observed one. Population model calculations are in accordance with the observed number ratios of novae below, within and above the period gap, but they are not able to reproduce the rather narrow peak observed at 3–4 h. Instead, they predict a more flat distribution in the range 3 h $\leq P_{\rm orb} \leq$ 6–8 h. This implies that the prescription usually used for AML due to magnetic braking in CVs above the period gap might not be correct.

Finally, we would like to mention that a new generation of terrestrial survey telescopes will soon come into operation, for instance the Vera C. Rubin Observatory (previously referred to as the Large Synoptic Survey Telescope, LSST), which will observe a large portion of the entire sky every ∼3 d, (a similar cadence as our CTIO set) revealing crucial information on the behaviour of many not yet observed, or even not yet identified old novae. This way, we will finally obtain better statistics on the orbital period distribution and other unsolved questions addresses here, but still open.

ACKNOWLEDGEMENTS

We are grateful to John Thorstensen for his detailed and valuable report. We thank Maja Vučković for suggestions related to the nova XX Tau. We give thanks to the European Southern Observatory (ESO) for the following observing runs in service mode: 087.D-0323(A), 088.D-0588(A), and 0102.D-0488(A). For RW UMi we give thanks to the Gran Telescopio Canarias (GTC) for the observing run GTC36-15A. IFM thanks to Comisión Nacional de Investigación Científica y Tecnológica, Programa Formación de Capital Humano Avanzado (CONICYT-PFCHA) Doctorado Nacional 2017-21171099 for doctoral fellowship. CT and NV acknowledge support from Fondo Nacional de Desarrollo Científico y Tecnológico (FONDECYT) grant number 1170566. MZ acknowledges support from CONICYT PAI (Concurso Nacional de Inserción en la Academia 2017, Folio 79170121) and CONICYT/FONDECYT (Programa de Iniciación, Folio 11170559). MRS acknowledges financial support from FONDECYT grant number 1181404 and the Núcleo de Formación Planetaria (NPF).

DATA AVAILABILITY

The data underlying this article are available in the appendix section. The photometric data and the spectroscopic measurements are available in its online supplementary material.

REFERENCES

Ak T., Retter A., Liu A., 2005, Publ. Astron. Soc. Aust., 22, 298
Andronov N., Pinsonneault M., Sills A., 2003, ApJ, 582, 358
Appenzeller I. et al., 1998, Messenger, 94, 1
Bailer-Jones C. A. L., 2015, PASP, 127, 994
Balman Ş., Yılmaz A., Retter A., Saygaç T., Esenoglu H., 2005, MNRAS, 356, 773
Balman Ş., Retter A., Bos M., 2006, AJ, 131, 2628
Balman S., Nasiroglu I., Akyuz A., 2009, Astron. Telegram, 2137, 1
Baptista R., Jablonski F. J., Cieslinski D., Steiner J. E., 1993, ApJ, 406, L67
Beardmore A. P. et al., 2012, A&A, 545, A116
Becker F., 1929, Astron. Nachr., 237, 71
Belloni D., Schreiber M. R., Pala A. F., Gänsicke B. T., Zorotovic M., Rodrigues C. V., 2020, MNRAS, 491, 5717
Bianchini A., Alford B., Canterna R., Della Valle M., 2001, MNRAS, 321, 625
Bianchini A., Tappert C., Canterna R., Tamburini F., Osborne H., Cantrell K., 2003, PASP, 115, 811
Bianchini A., Saygac T., Orio M., Della Valle M., Williams R., 2012, A&A, 539, A94
Bruch A. et al., 2019, New Astron., 67, 22
Buzzoni B. et al., 1984, Messenger, 38, 9
Campbell R. D., Shafter A. W., 1995, ApJ, 440, 336
Cepa J., 1998, Ap&SS, 263, 369
Chambers K. C. et al., 2016, preprint (arXiv:1612.05560)
Chen H.-L., Woods T. E., Yungelson L. R., Gilfanov M., Han Z., 2016, MNRAS, 458, 2916
Chochol D., Shugarov S. Y., Volkov I. M., Goranskij V. P., Metlova N. V., Barsukova E. A., Gabdeev M. M., 2013, Inf. Bull. Var. Stars, 6045, 1
Chochol D., Shugarov S., Pribulla T., Volkov I., 2014, Contrib. Astron. Obs. Skalnate Pleso, 43, 330
Collazzi A. C., Schaefer B. E., Xiao L., Pagnotta A., Kroll P., Löchel K., Henden A. A., 2009, AJ, 138, 1846
Collins K. A., Kielkopf J. F., Stassun K. G., Hessman F. V., 2017, AJ, 153, 77
Cumming A., 2002, MNRAS, 333, 589
Dai Z., Qian S., 2010, New Astron., 15, 380
Dai Z. B., Qian S. B., 2009, A&A, 503, 883
Diaz M. P., Bruch A., 1997, A&A, 322, 807
Diaz M. P., Steiner J. E., 1994, ApJ, 425, 252
Dobrotka A., Retter A., Liu A., 2006a, MNRAS, 371, 459
Dobrotka A., Friedjung M., Retter A., Hric L., Novak R., 2006b, A&A, 448, 1107
Downes R. A., Szkody P., 1989, AJ, 97, 1729

Downes R. A., Webbink R. F., Shara M. M., Ritter H., Kolb U., Duerbeck H. W., 2001, PASP, 113, 764
Downes R. A., Webbink R. F., Shara M. M., Ritter H., Kolb U., Duerbeck H. W., 2005, J. Astron. Data, 11, 2
Duerbeck H. W., 1981, PASP, 93, 165
Duerbeck H. W., 1987, Space Sci. Rev., 45, 1
Duerbeck H. W., 1992, MNRAS, 258, 629
Egan J. M., Woudt P. A., Warner B., Williams R. E., Steeghs D. T. H., Ribeiro V. A. R. M., 2014, in Woudt P. A., Ribeiro V. A. R. M., eds, ASP Conf. Ser. Vol. 490, Stellar Novae: Past and Future Decades. Astron. Soc. Pac., San Francisco, p. 67
Ferrario L., de Martino D., Gänsicke B. T., 2015, Space Sci. Rev., 191, 111
Finzell T. et al., 2018, ApJ, 852, 108
Flewelling H. A., et al., 2020, ApJS, 251 , 7
Fuentes-Morales I., Vogt N., Tappert C., Schmidtobreick L., Hambsch F.-J., Vučković M., 2018, MNRAS, 474, 2493
Gaia Collaboration et al., 2018, A&A, 616, A1
Gänsicke B. T. et al., 2009, MNRAS, 397, 2170
Gill C. D., O'Brien T. J., 1998, MNRAS, 300, 221
Goranskij V., Shugarov S., Zharova A., Kroll P., Barsukova E. A., 2010, Perem. Zvezdy, 30, 4
Goransky V. P., Shugarov S. Y., Dmitrienko E. S., Pavlenko E. P., 1997, in Maoz D., Sternberg A., Leibowitz E. M., eds, Astronomical Time Series, 218. p. 219
Hachisu I., Kato M., Nomoto K., 1996, ApJ, 470, L97
Hacke G., 1987, Inf. Bull. Var. Stars, 2979, 1
Haefner R., , 1999, Inf. Bull. Var. Stars, 4706, 1
Haefner R., Fiedler A., 2007, Inf. Bull. Var. Stars, 5751, 1
Henize K. G., 1967, ApJS, 14, 125
Hoffleit D., 1950, AJ, 55, 149
Honeycutt R. K., Robertson J. W., Turner G. W., 1998, AJ, 115, 2527
Honeycutt R. K., Kafka S., Jacobson H., Henden A. A., Hoffman D., Maxwell T., Robertson J. W., Croxall K., 2011a, AJ, 141, 122
Honeycutt R. K., Robertson J. W., Kafka S., 2011b, AJ, 141, 121
Howell S. B., Nelson L. A., Rappaport S., 2001, ApJ, 550, 897
Hurley J. R., Tout C. A., Pols O. R., 2002, MNRAS, 329, 897
Ingram D., Garnavich P., Green P., Szkody P., 1992, PASP, 104, 402
Kaluzny J., 1990, MNRAS, 245, 547
Kang T. W., Retter A., Liu A., Richards M., 2006a, AJ, 131, 1687
Kang T. W., Retter A., Liu A., Richards M., 2006b, AJ, 132, 608
Kato T., Ishioka R., Uemura M., Starkey D. R., Krajci T., 2004, PASJ, 56, S125
Katysheva N. A., Shugarov S. Y., 2007, in Napiwotzki R., Burleigh M. R., eds, ASP Conf. Seri. Vol. 372, 15th European Workshop on White Dwarfs. Astron. Soc. Pac., San Francisco, p. 523
Kawaler S. D., 1988, ApJ, 333, 236
King A. R., Kolb U., 1995, ApJ, 439, 330
Knigge C., 2006, MNRAS, 373, 484
Knigge C., Baraffe I., Patterson J., 2011, ApJS, 194, 28
Kouwenhoven M. B. N., Brown A. G. A., Goodwin S. P., Portegies Zwart S. F., Kaper L., 2009, A&A, 493, 979
Kroupa P., Tout C. A., Gilmore G., 1993, MNRAS, 262, 545
Kuerster M., Barwig H., 1988, A&A, 199, 201
Lipkin Y. M., Leibowitz E. M., 2008, MNRAS, 387, 289
Marin E., Shafter A. W., 2009, PASP, 121, 1090
Mason E. et al., 2013, MNRAS, 436, 212
Morales-Rueda L., Still M. D., Roche P., Wood J. H., Lockley J. J., 2002, MNRAS, 329, 597
Mróz P. et al., 2015, ApJS, 219, 26
Mróz P. et al., 2016, Nature, 537, 649
Munari U., Dallaporta S., Castellani F., Valisa P., Frigo A., Chomiuk L., Ribeiro V. A. R. M., 2013, MNRAS, 435, 771
Narloch W., Kaluzny J., Krzeminski W., Pych W., Rozyczka M., Shectman S., Thompson I. B., Tomov T., 2014, Balt. Astron., 23, 1
Nelson L. A., MacCannell K. A., Dubeau E., 2004, ApJ, 602, 938
Nogami D., Masuda S., Kato T., Hirata R., 1999, PASJ, 51, 115
Nomoto K., Nariai K., Sugimoto D., 1979, PASJ, 31, 287
Ochner P., Moschini F., Munari U., Frigo A., 2015, MNRAS, 454, 123
Olech A., 2002, Acta Astron., 52, 273
Pala A. F. et al., 2017, MNRAS, 466, 2855
Pala A. F. et al., 2020, MNRAS, 494, 3799
Pasquini L., Bonifacio P., Randich S., Galli D., Gratton R. G., 2004, A&A, 426, 651
Paunzen E., Vanmunster T., 2016, Astron. Nachr., 337, 239
Pavlenko E. P. et al., 2018, MNRAS, 479, 341
Peters C. S., Thorstensen J. R., 2006, PASP, 118, 687
Pickering E. C., 1893, Astron. Nachr., 134, 181
Pickering E. C., 1895, Astron. Nachr., 139, 119
Popova E. I., Tutukov A. V., Yungelson L. R., 1982, Ap&SS, 88, 55
Rappaport S., Verbunt F., Joss P. C., 1983, ApJ, 275, 713
Retter A., Leibowitz E. M., 1995, Int. Astron. Union Circ., 6234, 3
Retter A., Leibowitz E. M., 1998, MNRAS, 296, L37
Retter A., Lipkin Y., 2001, A&A, 365, 508
Retter A., Leibowitz E. M., Kovo-Kariti O., 1998, MNRAS, 293, 145
Retter A., Leibowitz E. M., Naylor T., 1999a, MNRAS, 308, 140
Retter A., Liller W., Garradd G., 1999b, IAU Circ., 7124, 3
Ringwald F. A., Chase D. W., Reynolds D. S., 2005, PASP, 117, 1223
Ritter H., Kolb U., 2003a, A&A, 404, 301
Ritter H., Kolb U., 2003b, A&A, 404, 301
Rodríguez-Gil P. et al., 2007, MNRAS, 377, 1747
Rodríguez-Gil P. et al., 2010, MNRAS, 407, L21
Rodríguez-Gil P., Torres M. A. P., 2005, A&A, 431, 289
Sana H., Gosset E., Evans C. J., 2009, MNRAS, 400, 1479
Schaefer B. E., 2018, MNRAS, 481, 3033
Schmidtobreick L., Tappert C., Bianchini A., Mennickent R. E., 2005, A&A, 432, 199
Schmidtobreick L., Shara M., Tappert C., Bayo A., Ederoclite A., 2015, MNRAS, 449, 2215
Schreiber M. R., Gänsicke B. T., 2001, A&A, 375, 937
Schreiber M. R., Gänsicke B. T., Cannizzo J. K., 2000, A&A, 362, 268
Schreiber M. R., Zorotovic M., Wijnen T. P. G., 2016, MNRAS, 455, L16
Shafter A. W., Misselt K. A., Veal J. M., 1993, PASP, 105, 853
Shafter A. W., Misselt K. A., Szkody P., Politano M., 1995, ApJ, 448, L33
Shapley H., 1921, Harvard College Obs. Bull., 760, 1
Shara M. M. et al., 2007, Nature, 446, 159
Shara M. M. et al., 2017, Nature, 548, 558
Shara M. M., Moffat A. F. J., McGraw J. T., Dearborn D. S., Bond H. E., Kemper E., Lamontagne R., 1984, ApJ, 282, 763
Shara M. M., Livio M., Moffat A. F. J., Orio M., 1986, ApJ, 311, 163
Shara M. M., Mizusawa T., Zurek D., Martin C. D., Neill J. D., Seibert M., 2012a, ApJ, 756, 107
Shara M. M., Mizusawa T., Wehinger P., Zurek D., Martin C. D., Neill J. D., Forster K., Seibert M., 2012b, ApJ, 758, 121
Shara M. M., Prialnik D., Hillman Y., Kovetz A., 2018, ApJ, 860, 110
Smak J., 2010, Acta Astron., 60, 357
Smith D. A., Dhillon V. S., Marsh T. R., 1998, MNRAS, 296, 465
Somers M. W., Mukai K., Naylor T., 1996, MNRAS, 278, 845
Swierczynski E. et al., 2010, in Prša A., Zejda M., eds, ASP Conf. Ser. Vol. 435, Binaries – Key to Comprehension of the Universe. Astron. Soc. Pac., San Francisco, p. 297
Szkody P., Ingram D., 1994, ApJ, 420, 830
Tamburini F., di Mille F., Bianchini A., Johnson P., 2007, A&A, 464, 697
Tappert C., Ederoclite A., Mennickent R. E., Schmidtobreick L., Vogt N., 2012, MNRAS, 423, 2476
Tappert C., Schmidtobreick L., Vogt N., Ederoclite A., 2013, MNRAS, 436, 2412
Tappert C., Vogt N., Della Valle M., Schmidtobreick L., Ederoclite A., 2014, MNRAS, 442, 565
Tappert C., Vogt N., Ederoclite A., Schmidtobreick L., Vučković M., Becegato L. L., 2020, A&A, 641, A122
Thorstensen J. R., Ringwald F. A., 1995, Inf. Bull. Var. Stars, 4249, 1
Thorstensen J. R., Taylor C. J., 2000, MNRAS, 312, 629

Thorstensen J. R., Peters C. S., Skinner J. N., 2010, PASP, 122, 1285
Thorstensen J. R., Ringwald F. A., Taylor C. J., Sheets H. A., Peters C. S., Skinner J. N., Alper E. H., Weil K. E., 2017, Res. Notes Am. Astron. Soc., 1, 29
Tomov T., Swierczynski E., Mikolajewski M., Ilkiewicz K., 2015, A&A, 576, A119
Townsley D. M., Bildsten L., 2004, ApJ, 600, 390
Townsley D. M., Bildsten L., 2005, ApJ, 628, 395
Townsley D. M., Gänsicke B. T., 2009, ApJ, 693, 1007
van Dokkum P. G., 2001, PASP, 113, 1420
Vogt N., Schreiber M. R., Hambsch F.-J., Retamales G., Tappert C., Schmidtobreick L., Fuentes-Morales I., 2017, PASP, 129, 014201
Vogt N., Tappert C., Puebla E. C., Fuentes-Morales I., Ederoclite A., Schmidtobreick L., 2018, MNRAS, 478, 5427
Walter F. M., 2015, in Dufour P., Bergeron P., Fontaine G., eds, ASP Conf. Se. Vol. 493, 19th European Workshop on White Dwarfs. Astron. Soc. Pac., San Francisco, p. 507
Walter F. M., Battisti A., Towers S. E., Bond H. E., Stringfellow G. S., 2012, PASP, 124, 1057
Warner B., 1986, MNRAS, 222, 11
Warner B., 2002, in Hernanz M., José J., eds, AIP Conf. Proc. Vol. 637, Classical Nova Explosions. Am. Inst. Phys., New York, p. 3
Warner B., 2003a, Cataclysmic Variable Stars
Warner B., 2003b, MNRAS, 62, 74
Warner B., Woudt P. A., 2002, PASP, 114, 1222
Warner B., Woudt P. A., 2009, MNRAS, 397, 979
Weight A., Evans A., Naylor T., Wood J. H., Bode M. F., 1994, MNRAS, 266, 761
Wood M. A., Still M. D., Howell S. B., Cannizzo J. K., Smale A. P., 2011, ApJ, 741, 105
Woudt P. A., Warner B., 2001, MNRAS, 328, 159
Woudt P. A., Warner B., 2002, MNRAS, 335, 44
Woudt P. A., Warner B., 2003, MNRAS, 340, 1011
Woudt P. A., Warner B., 2010, MNRAS, 403, 398
Woudt P. A., Warner B., Pretorius M. L., 2004, MNRAS, 351, 1015
Woudt P. A., Warner B., Spark M., 2005, MNRAS, 364, 107
Woudt P. A., Warner B., Osborne J., Page K., 2009, MNRAS, 395, 2177
Yaron O., Prialnik D., Shara M. M., Kovetz A., 2005, ApJ, 623, 398
Zacharias N., Monet D. G., Levine S. E., Urban S. E., Gaume R., Wycoff G. L., 2004, American Astronomical Society Meeting Abstracts, 205, 4815
Zemko P. et al., 2018, MNRAS, 480, 4489
Zengin Çamurdan D., İbanoğluC., Çamurdan C. M., 2010, New Astron., 15, 476
Zhao P., McClintock J. E., 1997, ApJ, 483, 899
Zorotovic M. et al., 2016, MNRAS, 457, 3867
Zorotovic M., Schreiber M. R., Gänsicke B. T., Nebot Gómez-Morán A., 2010, A&A, 520, A86
Zorotovic M., Schreiber M. R., Parsons S. G., 2014, A&A, 568, L9
Zwitter T., Munari U., 1994, A&AS, 107, 503

SUPPORTING INFORMATION

Supplementary data are available at *MNRAS* online.

Appendix (Tables).

Please note: Oxford University Press is not responsible for the content or functionality of any supporting materials supplied by the authors. Any queries (other than missing material) should be directed to the corresponding author for the article.

APPENDIX A: EXTRA MATERIAL

Individual light curves and spectra for the analysed novae are shown as extra material. The epochs for the eclipses and the orbital periods considered in this work are also presented in the follow tables.

Table A6. Eclipse epochs of the four eclipsing novae from the literature and from CTIO observation data. The O–C values refer to the ephemerides given in Table 5.

Object	E	HJD −2 400 000 d	O–C d	Ref.
WY Sge	−14178	44881.639	0.0018	(1)
	−14171	44882.711	−0.0017	(1)
	−14003	44908.524	0.0007	(1)
	−12510	45137.8998	0.0001	(1)
	−12498	45139.7434	0.0001	(1)
	11564	48836.4976	−0.0001	(2)
	11571	48837.5726	−0.0006	(2)
	14151	49233.9498	−0.0005	(2)
	14157	49234.8722	0.0001	(2)
	14170	49236.869	−0.0004	(2)
	14176	49237.791	−0.0002	(2)
	14177	49237.945	0.0002	(2)
	63241	56775.8667	−0.0035	(3)
	63306	56785.8580	0.0015	(3)
	63618	56833.7893	−0.0012	(3)
	63637	56836.7094	−0.0001	(3)
	63696	56845.7720	−0.0020	(3)
	63884	56874.6585	0.0013	(3)
	63942	56883.5697	0.0017	(3)
	65552	57130.9224	0.0028	(3)
V728 Sco	−14	56013.8704	0.0002	(4)
	−7	56014.8379	−0.0007	(4)
	0	56015.8073	0.0004	(4)
	29	56019.8182	−0.0005	(4)
	346	56063.6729	0.0008	(4)
	353	56064.6404	−0.0001	(4)
	354	56064.7750	−0.0010	(4)
	4988	56705.8401	0.0003	(3)
	5082	56718.8412	−0.0025	(3)
	5147	56727.8347	−0.0010	(3)
	5169	56730.8801	0.0010	(3)
	5234	56739.8729	0.0017	(3)
	5558	56784.6921	−0.0007	(3)
	6244	56879.5948	0.0017	(3)
	6446	56907.5382	0.0007	(3)
	6800	56956.5117	0.0023	(3)
	6865	56965.5034	0.0020	(3)
	7569	57062.8920	0.0002	(3)
	8154	57143.8197	−0.0001	(3)
	8709	57220.5947	−0.0031	(3)
	8804	57233.7386	−0.0014	(3)
OY Ara	−42829	49862.822	0.0001	(5)
	0	56516.5710	−0.0012	(3)
	283	56560.5463	−0.0009	(3)
	1160	56696.8211	−0.0022	(3)
	1289	56716.8686	0.0002	(3)
	1366	56728.8375	0.0041	(3)
V849 Oph	0	48799.7412	0.0000	(6)
	1	48799.9149	0.0009	(6)
	186	48831.8736	−0.0003	(6)
	191	48832.7384	0.0008	(6)
	29884	53962.3846	−0.0003	(7)
	29890	53963.4197	−0.0017	(7)
	29895	53964.2840	−0.0012	(7)
	44687	56519.6881	−0.0056	(3)
	46487	56830.6621	0.0074	(3)

Note. Ref: (1) Shara et al. (1984), (2) Somers, Mukai & Naylor (1996), (3) this work, (4) Tappert et al. (2013), (5) Zhao & McClintock (1997), (6) Shafter, Misselt & Veal (1993), (7) Zengin Çamurdan, İbanoğlu & Çamurdan (2010)

Table A7. The orbital periods of old novae considered to create the distribution shown in Fig. 10. The name, P_{orb}, the method used to derived it and the references are presented (OM: photometric orbital modulation, RV: Radial velocity, E: eclipse and SH: superhump). Those novae with daily alias ambiguities are categorized as 'provisional' and they are marked with ∗. The choice for the orbital period value presented here is discussed in Section 5.

Name	P_{orb}(d)	Method	Reference	Name	P_{orb}(d)	Method	Reference
RW UMi	0.05912	OM-RV	(1), (2), This paper	V2467 Cyg	0.1596	OM	(34)
GQ Mus	0.059365	OM-RV	(3), (4)	DO Aql	0.167762	E	(35)
CP Pup	0.061264	OM-RV-SH	(5), (6)	V849 Oph	0.17275611	E	(35), This paper
IL Nor*	0.06709	OM	This paper	V697 Sco	0.187	OM	(36)
V458 Vul	0.068126	RV	(7)	V825 Sco	0.19165877	E	(16)
V1974 Cyg	0.08126	OM-SH	(8)	DQ Her	0.193621	E-RV	(37)
RS Car*	0.082429	OM-SH?	(9), This paper	CT Ser	0.195	RV	(38)
DD Cir	0.09746	E	(10)	AT Cnc	0.201634	RV-OM	(39), (40), (41)
V Per	0.107123	E-RV	(11)	T Aur	0.204378	E	(42)
V597 Pup	0.11119	E	(12)	V446 Her	0.207	RV	(29)
QU Vul	0.111765	E	(13)	V4745 Sgr	0.20782	OM	(43)
CQ Vel*	0.11272	OM-RV	This paper	HZ Pup	0.212	RV	(44)
V2214 Oph	0.117515	OM	(14)	AP Cru	0.213	OM	(9)
V630 Sgr	0.11793	E-SH	(15), (16)	AR Cir	0.214	OM-RV	(22)
V351 Pup	0.1182	OM	(15)	HR Del	0.214165	RV	(45)
V5116 Sgr	0.1238	E	(16)	V5588 Sgr	0.214321	OM	(16)
V4633 Sgr	0.1255667	OM-SH	(16), (17)	NR TrA	0.219	E-RV	(46)
V363 Sgr	0.126066	OM	This paper	CN Vel	0.2202	RV	(22)
DN Gem	0.127844	RV	(18), (19)	V365 Car	0.223692	OM-RV	(22), This paper
V339 Del	0.1314	OM	(20)	V1039 Cen	0.247	OM	(47)
V4742 Sgr	0.1336159	E	(16)	V1425 Aql	0.2558	OM	(48)
V1494 Aql	0.134614	E	(21)	HS Pup	0.2671	RV	(22)
V5585 Sgr	0.137526	E	(16)	V2615 Oph	0.272339	OM	(16)
V603 Aql	0.138201	OM-RV-SH	(18)	V4743 Sgr	0.2799	OM	(49)
V728 Sco	0.13833866	E-RV	(22), This paper	V972 Oph	0.281	RV	(22)
V1668 Cyg	0.1384	E	(23)	BY Cir	0.2816	E	(10)
XX Tau*	0.13588	RV	This paper	V2540 Oph	0.284781	OM	(50)
DY Pup	0.13952	E	This paper	V1059 Sgr	0.2861	RV	(51)
V1500 Cyg	0.139613	OM	(24)	Z Cam	0.289841	RV	(52), (53)
RR Cha	0.1401	E-SH	(9)	V959 Mon	0.29585	OM	(54)
V909 Sgr	0.14286	OM-RV	(22)	V838 Her	0.297635	E	(55)
RR Pic	0.145025959	OM-SH	(25), (26)	V2275 Cyg	0.3145	OM	(56)
CP Lac	0.145143	RV	(18)	BT Mon	0.333814	E-RV	(57)
V500 Aql	0.1452	OM-RV	(27), (11)	V2677 Oph	0.3443	OM	(16)
V2468 Cyg	0.14525	OM	(28)	QZ Aur	0.357496	E-RV	(58), (59)
V533 Her	0.147	RV	(29)	Q Cyg	0.42036	RV	(16)
V2574 Oph	0.1477	OM-SH	(30)	J17014 4306	0.5340257	E	(60)
V5113 Sgr	0.150015	OM	(16)	V841 Oph	0.601304	RV	(18)
V4579 Sgr	0.15356146	E	(16)	V368 Aql	0.690509	E	(61)
V992 Sco	0.15358	OM	(10)	V723 Cas	0.693277	OM	(62)
V373 Sct	0.1536	RV	(22)	CP Cru	0.944	E	(10)
WY Sge	0.153634547	E	(31), This paper	V2674 Oph	1.30207	E	(16)
X Cir	0.15445953	E	This paper	X Ser	1.48	RV	(29)
OY Ara	0.155390	E-RV	(32), This paper	V5589 Sgr	1.5923	E	(16)
V1493 Aql	0.156	OM	(33)	HV Cet	1.772	OM	(63)
V2572 Sgr*	0.156215	OM-RV	This paper	GK Per	1.996803	RV	(64)

Note. References: (1) Retter & Lipkin (2001), (2) Bianchini et al. (2003), (3) Diaz & Steiner (1994), (4) Narloch et al. (2014), (5) Mason et al. (2013), (6) Bianchini et al. (2012), (7) Rodríguez-Gil et al. (2010), (8) Olech (2002), (9) Woudt & Warner (2002), (10) Woudt & Warner (2003), (11) Haefner & Fiedler (2007), (12) Warner & Woudt (2009), (13) Shafter et al. (1995), (14) Baptista et al. (1993), (15) Woudt & Warner (2001), (16) Mróz et al. (2015), (17) Lipkin & Leibowitz (2008), (18) Peters & Thorstensen (2006), (19) Retter, Leibowitz & Naylor (1999a), (20) Chochol et al. (2014), (21) Kato et al. (2004), (22) Tappert et al. (2013), (23) Kaluzny (1990), (24) Pavlenko et al. (2018), (25) Vogt et al. (2017), (26) Fuentes-Morales et al. (2018), (27) Haefner (1999), (28) Chochol et al. (2013), (29) Thorstensen & Taylor (2000), (30) Kang et al. (2006a), (31) Somers et al. (1996), (32) Zhao & McClintock (1997), (33) Dobrotka et al. (2006b), (34) Swierczynski et al. (2010), (35) Shafter et al. (1993), (36) Warner & Woudt (2002), (37) Dai & Qian (2009), (38) Ringwald, Chase & Reynolds (2005), (39) Nogami et al. (1999), (40) Shara et al. (2012b), (41) Bruch et al. (2019), (42) Dai & Qian (2010), (43) Dobrotka, Retter & Liu (2006a), (44) Thorstensen et al. (2017), (45) Kuerster & Barwig (1988), (46) Walter (2015), (47) Woudt et al. (2005), (48) Retter, Leibowitz & Kovo-Kariti (1998), (49) Kang et al. (2006b), (50) Ak, Retter & Liu (2005), (51) Thorstensen, Peters & Skinner (2010), (52) Thorstensen & Ringwald (1995), (53) Shara et al. (2007), (54) Munari et al. (2013), (55) Ingram et al. (1992), (56) Balman et al. (2005), (57) Smith, Dhillon & Marsh (1998), (58) Szkody & Ingram (1994), (59) Campbell & Shafter (1995), (60) Shara et al. (2017), (61) Marin & Shafter (2009), (62) Ochner et al. (2015), (63) Beardmore et al. (2012), (64) Morales-Rueda et al. (2002)

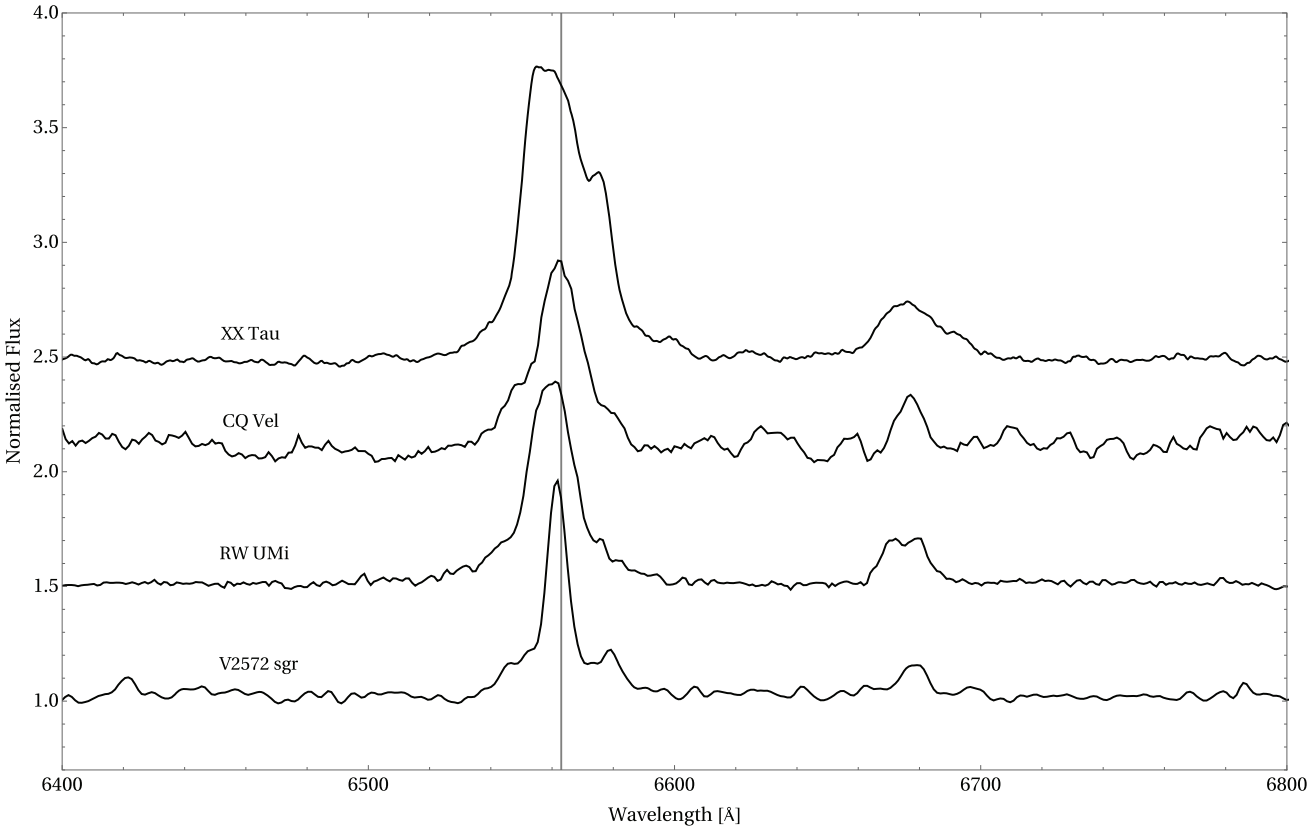

Figure A1. Normalized average spectrum for V2572 Sgr, RW UMi, CQ Vel, and XX Tau for which radial velocities were measured from the Hα emission line. The grey line marks the central lambda of Hα. The λ6678 Å He I emission line is also present in all spectra.

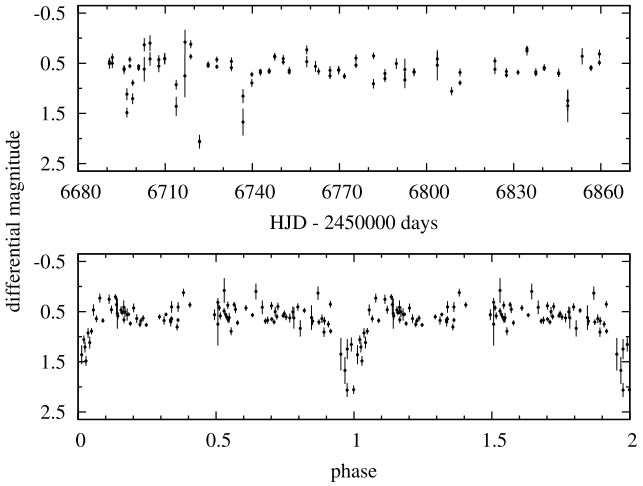

Figure A2. Top: The CTIO light curve of X Cir. Bottom: Phase light curve of this data according to ephemeris (5) described in Section 3.3.

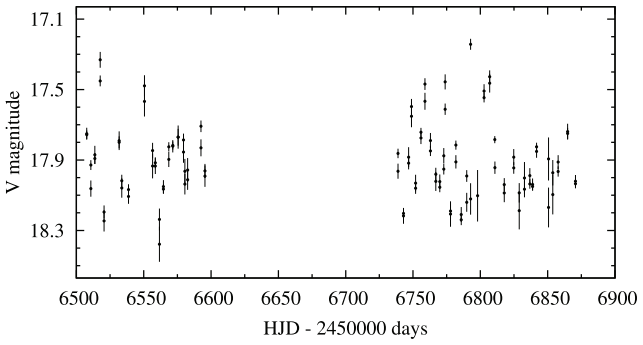

Figure A3. The CTIO light curves of V2572 Sgr described in Section 3.7.

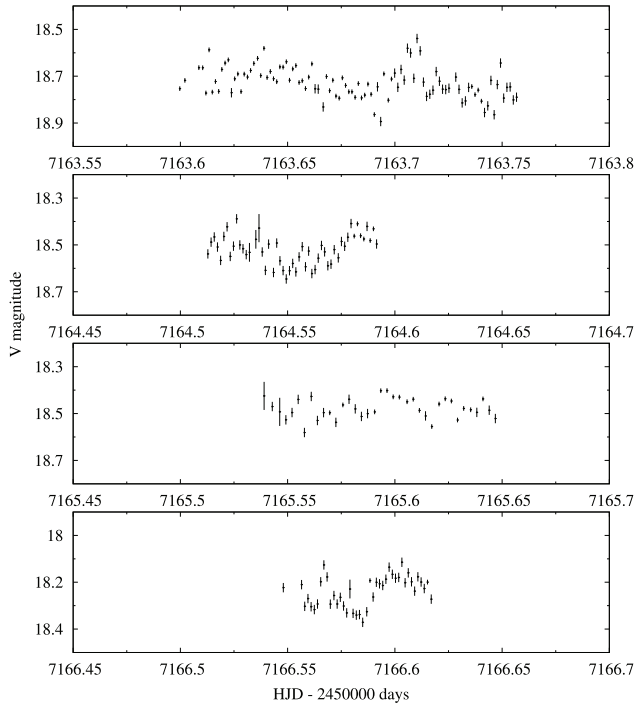

Figure A4. *V*-band light curves of IL Nor taken in 2015 at du Pont telescope.

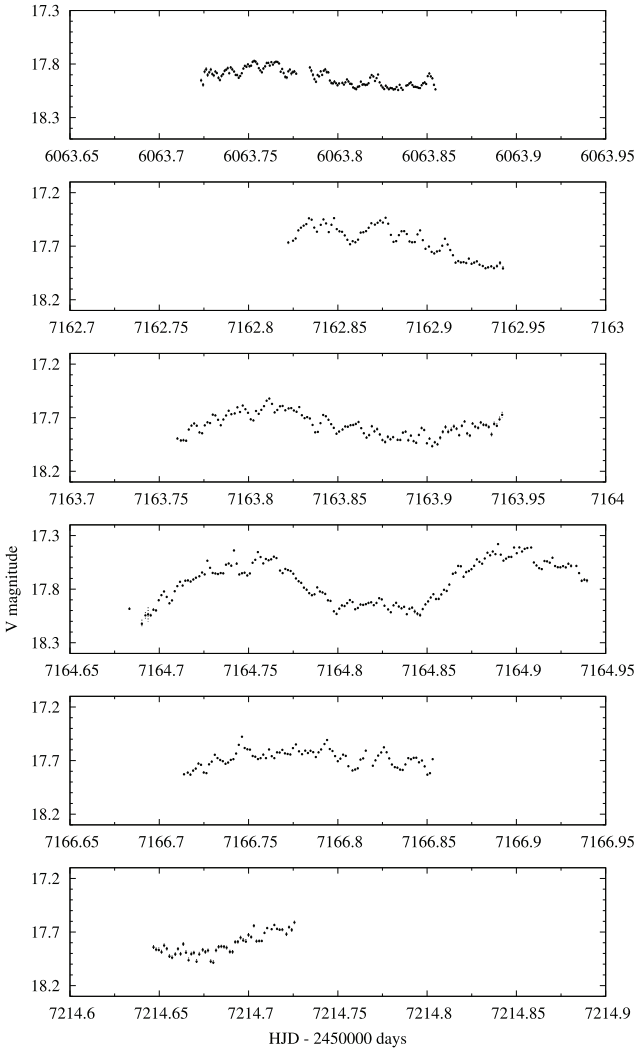

Figure A5. *V*-band light curves of V2572 Sgr. The first one was observed with EFOSC2/NTT in May 2012 and the other ones with du Pont telescope in 2015 May–July.

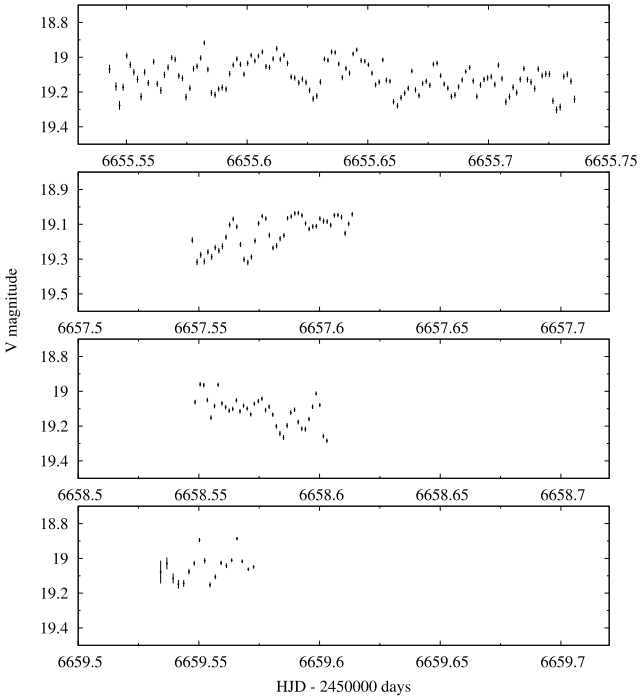

Figure A6. Light curves of XX Tau taken at du Pont telescope.

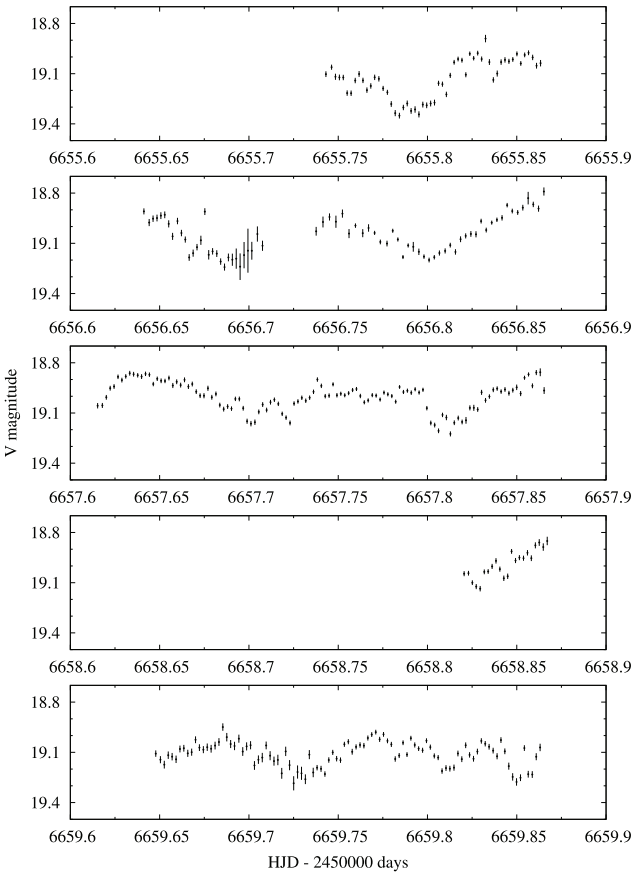

Figure A7. *V*-band light curves of CQ Vel taken at du Pont telescope.

This paper has been typeset from a TEX/LATEX file prepared by the author.